NATURAL GAMMA ACTIVITIES IN GLACIMARINE SEDIMENTS: CORRELATIONS WITH TERRESTRIAL SOURCE DATA

By

ALICE HILDICK

A THESIS PRESENTED TO THE GRADUATE SCHOOL
OF THE UNIVERSITY OF FLORIDA IN PARTIAL FULFILLMENT
OF THE REQUIREMENTS FOR THE DEGREE OF
MASTER OF SCIENCE

UNIVERSITY OF FLORIDA

2006

To those who endured it with me

ACKNOWLEDGMENTS

First, I would like to thank Dr. John Jaeger for his patience and help throughout the entire project. I would also like to thank those on the R/V Alpha Helix science crew who did the sampling for this study, and to Gillian Rosen for her countless hours of consult. I would like to thank Dr. Mike Perfit and Warren Grice for their help with petrographic analysis, and Dr. Guerry McClellan for help with XRD analysis. A special thank you goes to my family, friends, and those at Geohazards, Inc. for their support throughout this process. Lastly I want to give a sincere thank you to Scott Purcifull and Nicole Yonke, without whom this project never would have been finished.

TABLE OF CONTENTS

LIST OF TABLES

LIST OF FIGURES

Abstract of Thesis Presented to the Graduate School
of the University of Florida in Partial Fulfillment of the
Requirements for the Degree of Master of Science

NATURAL GAMMA ACTIVITIES IN GLACIMARINE SEDIMENTS: CORRELATIONS WITH TERRESTRIAL SOURCE DATA

By

Alice Hildick

December 2006

Chair: John M. Jaeger
Major Department: Geology

The provenance analysis of fine-grained sediments is particularly important in continental margin environments where fine particles dominate the stratigraphic record. One area receiving voluminous quantities of fine-grained material is the tectonically active southern Alaska margin, where sediment derived by glacial erosion is accumulating at some of the highest rates globally. Although the magnitude and rate of sediment delivery is known, little work has been done to determine the terrestrial sources and surficial processes responsible for spatial heterogeneities in accumulation patterns.

Natural gamma activities (^{238}U, ^{232}Th, and ^{40}K) and mineralogy of two cores were examined at differing locations within the Gulf of Alaska (GOA) in an attempt to distinguish them using only these techniques. Cores were chosen based on their differing lithologies, one core being comprised of material derived entirely from the Valdez Group of the Chugach terrane, the other being comprised entirely of material from the Yakataga Formation (a ~5km thick marine and glacimarine clastic deposit of unknown origin). Natural gamma activities were measured on a Canberra UltraLow Background Planar-Style germanium detector, mineralogy was determined by both XRD and petrographic analyses. In addition to bulk sample analysis, samples were separated into sand-, silt- and clay-sized fractions to examine the association of

grain size and radioistopic activity. Elemental concentrations of ^{238}U, ^{232}Th and ^{40}K were compared to published geochemical river and stream sediment data.

Measurements in this study fall well within ranges of parent source material, revealing their accuracy as a provenance tool. Radioisotopic activity measurements from each size fraction reveal an association of ^{238}U, ^{232}Th, and ^{40}K with the fine-sized fraction, particularly of ^{40}K with clay-sized fraction. The similarity between both natural gamma activities and mineralogy between cores suggest that sediments of both cores have the same source material. The Valdez Group is a well-established member of the Chugach terrane, implying that the glacially-derived sediments of the Yakataga Formation are also derived for the Chugach terrane.

CHAPTER 1
INTRODUCTION

Sediment source (provenance) identification is important in geological and environmental management fields for basin analysis. It is an important tool in tectonic reconstructions and in understanding weathering and transport processes, which help shape the topography observed today. Sediment provenance is used to constrain the sedimentary processes from erosion to final deposition, with the goal being to reconstruct parent-rock assemblages of sediments and the climatic and physiographic conditions under which these sediments formed (Augustsson, Fanning, Munker, Bahlburg, and Jacobsen 2003; Weltje and Eynatten 2004). The provenance analysis of fine-grained sediments is particularly important in continental margin environments, where these fractions dominate the stratigraphic record. One area receiving voluminous quantities (~250 x 10^6 tons/y; Jaeger, Nittrouer, Scott, and Milliman 1998) of fine-grained material is the Gulf of Alaska (GOA) margin, where sediment derived by glacial erosion is rapidly accumulating (Figure 1-1). Although the magnitude and rate of sediment delivery is known, there has been little provenance work done to determine the terrestrial sources and surficial processes responsible for the spatial heterogeneities in accumulation patterns.

Geochemical characteristics of sedimentary rocks are known to provide important clues to their provenance and depositional environments. During the last few decades, geochemical study of sedimentary rocks has grown, particularly in the area of provenance and source composition investigations (McLennan, Taylor, and Kroner 1983; Fedo, Eriksson, and Krogstad 1996; Kampunzu, Cailteux, Moine, and Loris 2005). Many provenance studies focus on sand fractions or bulk sediment samples, with heavy mineral analysis and rare earth element (REE) patterns being the dominant “fingerprinting” techniques applied (Basu 2002; Kampunza et al. 2005; Kairyte, Stevens, and Egidijus 2005; Nyakairu and Koeberl 2001). Single grain

techniques are used, but are only effective if their results can be firmly connected to the bulk mass transfer (Andersen 2004; Kairyte et al. 2005). Other criteria employed to identify sources include detrital thermochronology (using zircons or apatite), bulk composition analysis, and analysis of magnetic properties (Boggs 2001; Hounslow and Morton 2004; Liu, Zhu, and Li 2003; Watkins and Maher 2003). Sediments from many depositional environments, however, do not contain enough sand to make statistically significant petrographic determinations. Geochemical approaches to sedimentary provenance analysis are therefore especially useful where coarse sediment is scarce (McDaniel, McLennan, and Hanson 1997; Andrews and Principato 2002; Kairyte et al. 2005).

Whereas REE and other trace elemental analyses are a preferred method of studying the provenance of fine-grained sediments (Basu 2002; Weltje and Eynatten 2004), they are time-consuming and expensive, and thus are not ideal for higher spatial resolution studies of sediment cores. For decades, the oil industry has used several wire-line logging tools (e.g., spectral gamma ray, photoelectric index) to provide high-resolution, continuous proxies of elemental abundances and mineralogy (Doveton 1994). Recently, Carter and Gammon (2004) used continuous gamma-ray spectroscopy on cores from ODP site 1119 on the Canterbury Margin of New Zealand to show climatically controlled variability in the delivery of fine-grained ^{40}K-rich glacial rock flour from the Southern Alps. Geochemical provenance studies have been successful in using isotopic data to determine provenance and paleoclimate (Lang Farmer, Ayuso, and Plafker 1993; Schnyder, Deconick, and Boudin 2005) and fine-grained sediments have proved to record accurately global paleoclimate evolution (Fabres, Calafat, Canals, Barcena, and Flores 2000).

Southern Alaska has been referred to as an *in situ* natural laboratory to study the interaction of glacial and orogenic processes, tectonics, and continental margin sedimentation

(Jaeger et al. 2001). The focus of this research is to use geochemical data at two separate locations (Figs. 1-2 and 1-3) within the GOA region to determine (1) if grain-size and/or mineralogy plays a role in controlling naturally occurring radioisotopic activities (^{238}U, ^{232}Th, ^{40}K), and (2) the ability of these data to differentiate between two unique terranes in order to establish provenance. Detailed fluvial sediment geochemical data from stream and river sediment samples is available for comparison (Weaver 1983). (Figs. 1-4 through 1-6) Also available is an aeroradiometric survey map (Saltus, Riggle, Clark, and Hill 1999). (Figure 1-7)

The hypothesis is that ^{238}U is associated with zircons and heavy minerals being carried predominantly in the coarse (>63μm) fraction, and ^{232}Th and ^{40}K are concentrated in the fine-sized fraction due to the presence of clays (illite, chlorite) and mica. If this is true, then bulk rocks within the source area for core 249PC (which is composed of more fine-grained, metasedimentary, flysch material of the Valdez Group) should contain lower ^{238}U values and higher ^{232}Th and ^{40}K. The data from core 223BC should contain more coarse material (from the Yakataga Formation) and, therefore, contain higher levels of uranium relative to potassium and thorium. Other factors such as clay mineralogy and diagenesis are expected to play a role in radioisotopic activity, but will be minimal relative to grain size. If grain size does in fact play a role in controlling radioisotopic activities, then it could be possible to determine provenance based on this technique.

Core location is important due to possible influences from other sources, such as changes in clay mineralogy, which might change the geochemical signature. The two cores selected are each sourced by only one drainage basin. Core 223BC was taken 4 km from the ice front in Icy Bay, and core 249PC was taken just outside the mouth of Resurrection Bay near the termination of Bear Glacier. Based on core locations and associated drainage basins, material associated

with a source other than the Yakataga Formation for core 223BC or the Valdez Group for core 249PC is minimal. (Figure. 1-7)

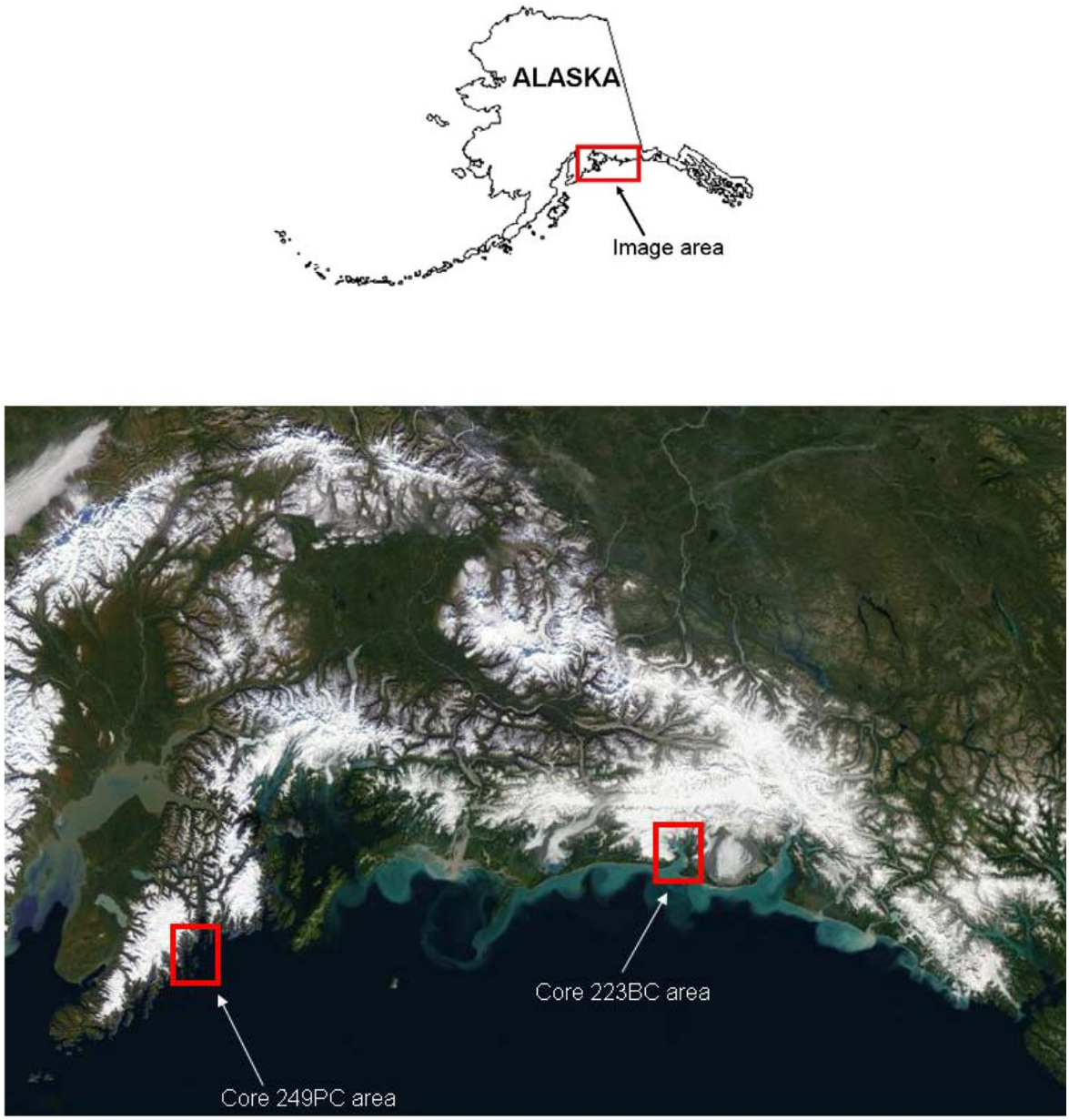

Figure 1-1. Satellite image of Alaska coastal margin showing extent of glaciation and sample environments (modified from MODIS Rapid Response Project at NASA/GSFC, Gulf of Alaska Science Plan 2004).

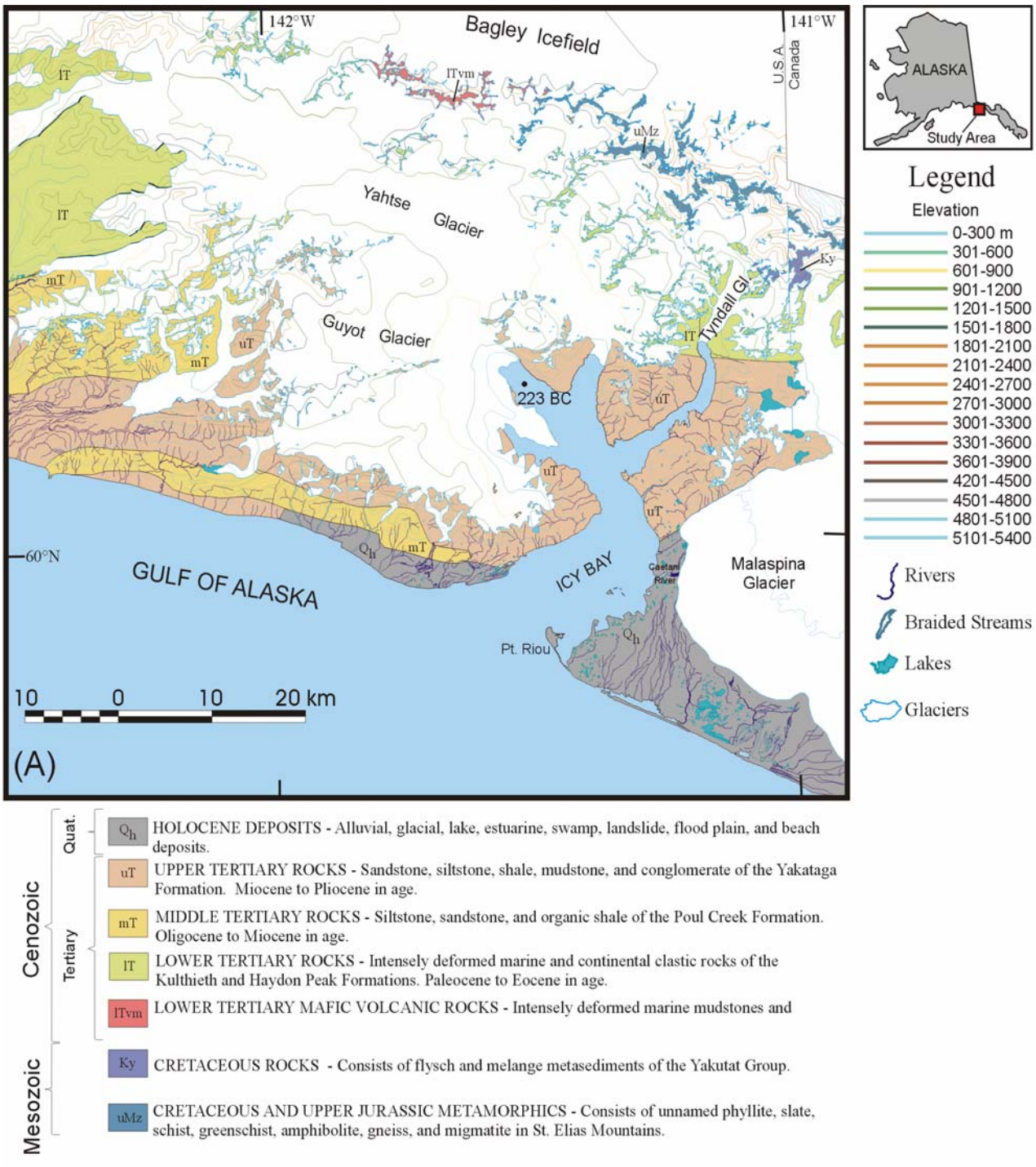

Figure 1-2. Location and geological map of area surrounding core 223BC. Sediments within core 223BC are sourced by the Guyot Glacier (courtesy of John Jaeger).

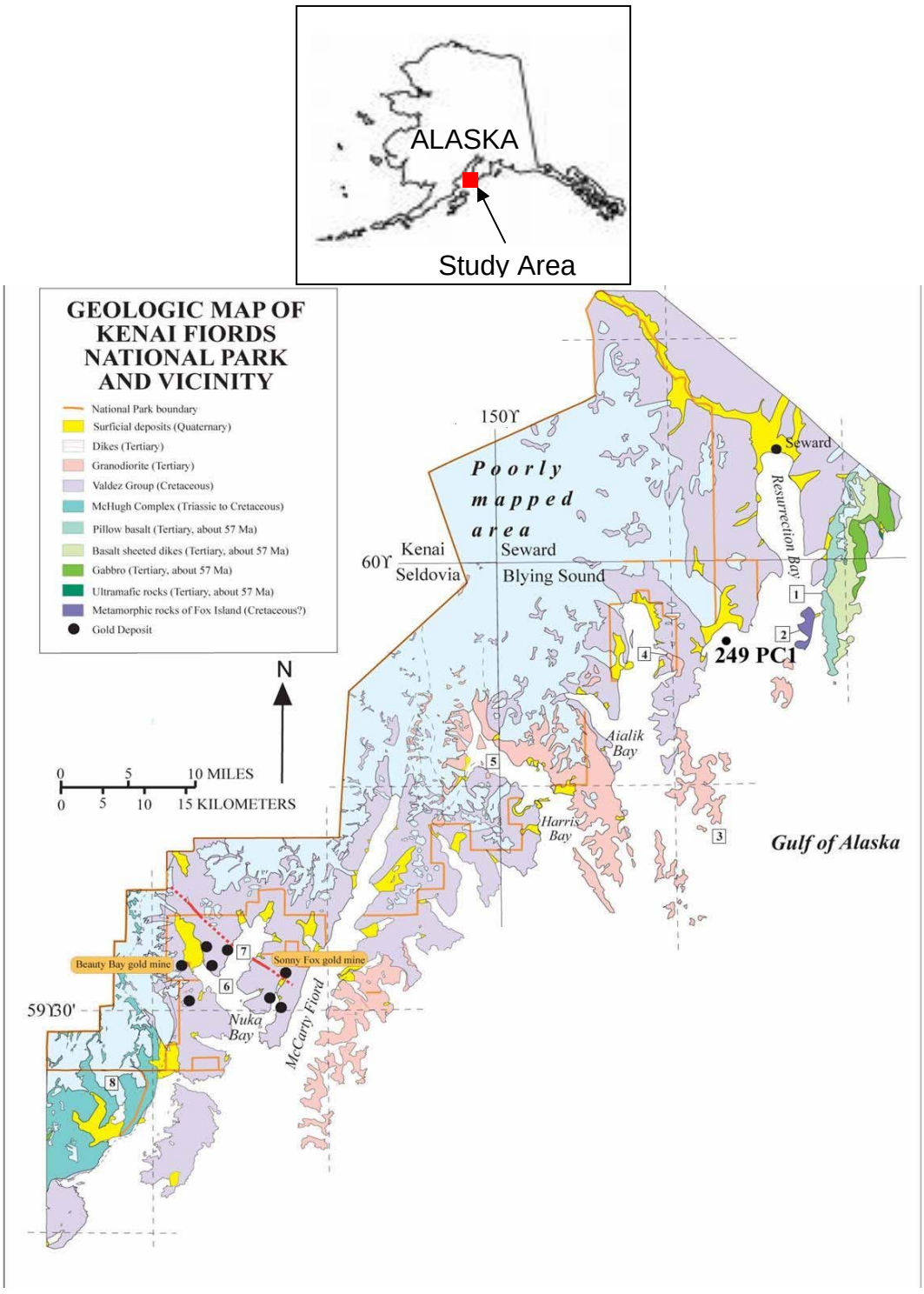

Figure 1-3. Location and geological map of area surrounding core 249PC. The core contains sediment sourced from Bear Glacier (modified from Bradley and Donley 1995, USGS).

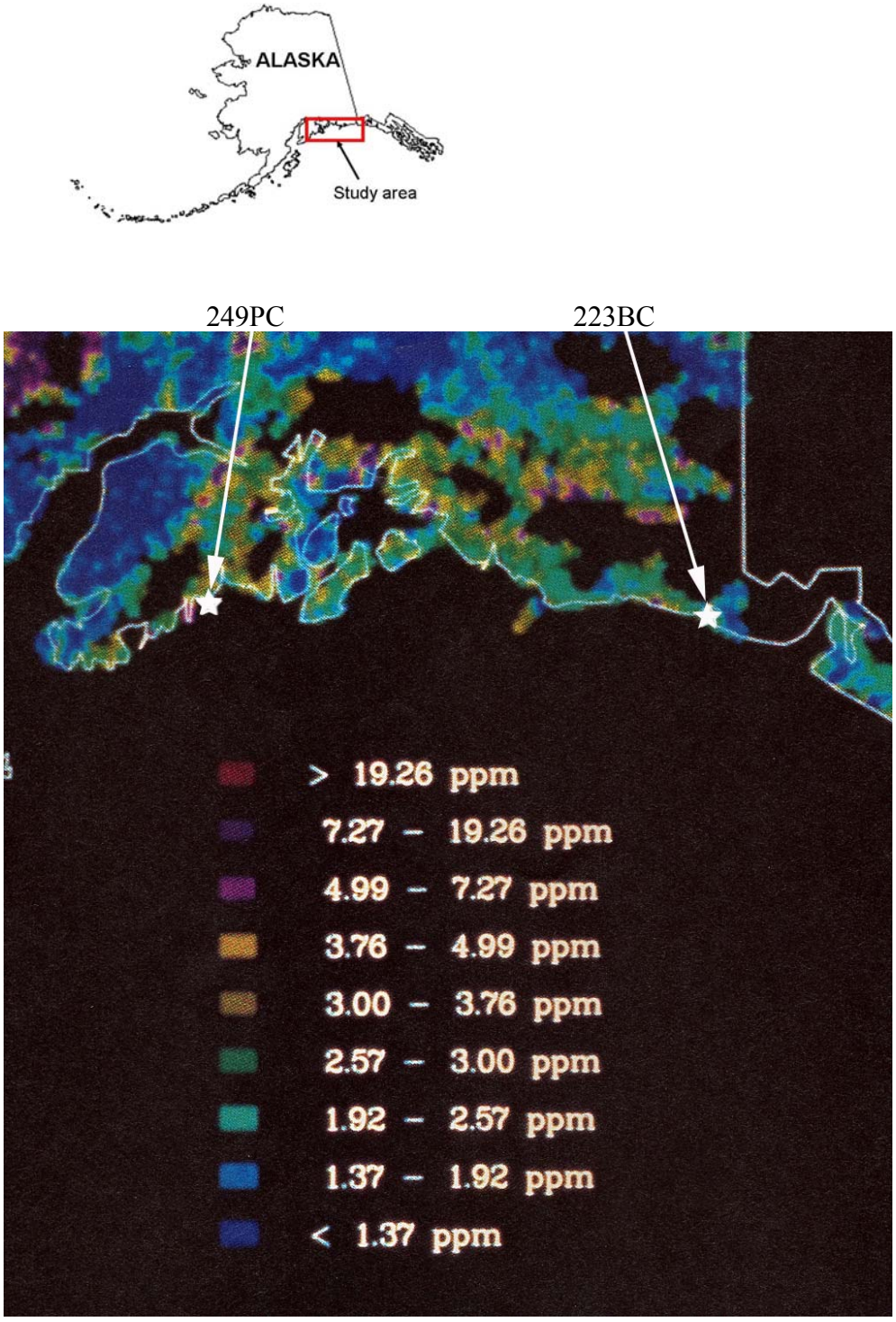

Figure 1-4. Published uranium geochemical data in southern Alaska from lake and river sediment samples (modified from Weaver 1983).

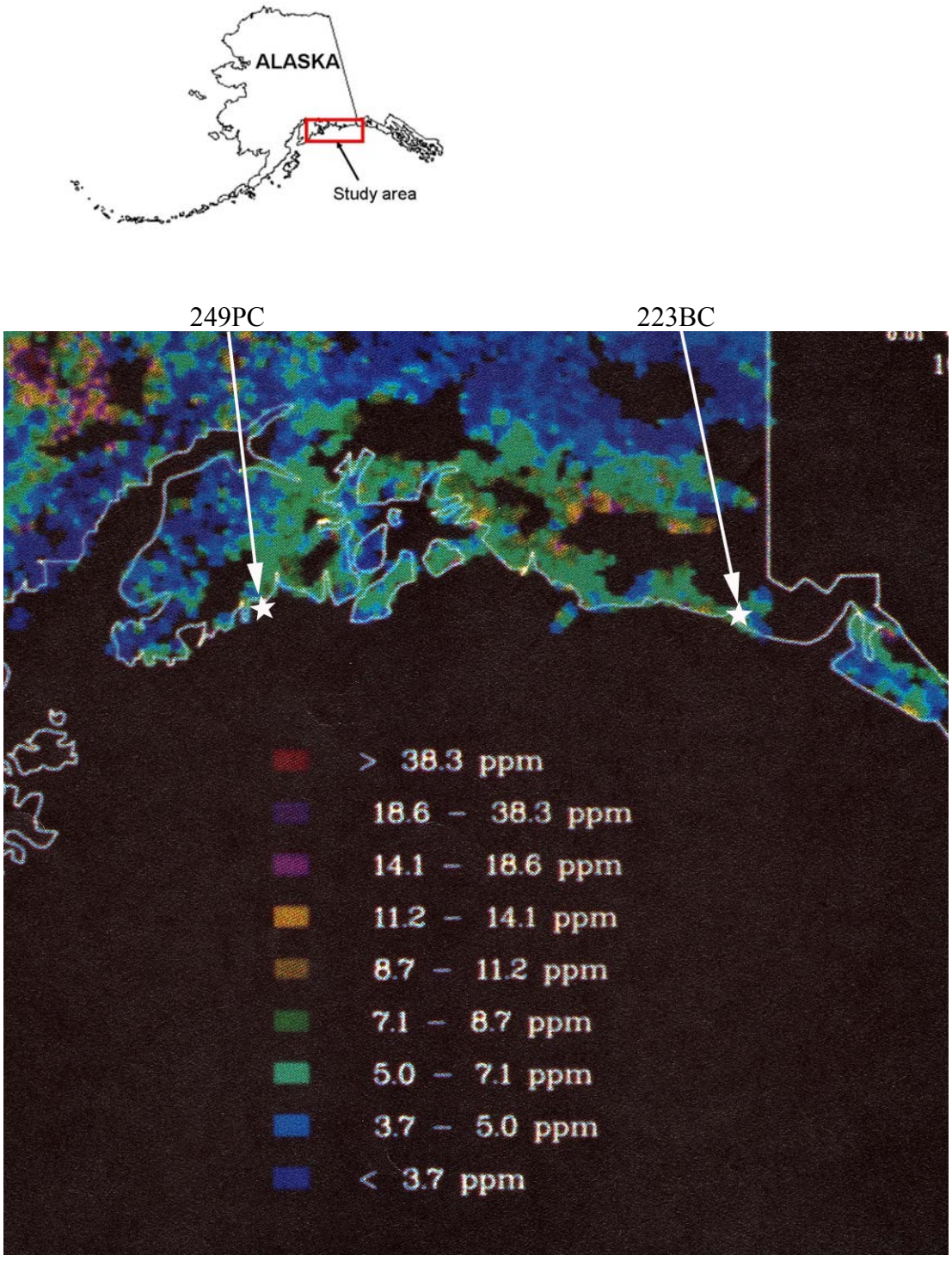

Figure 1-5. Published thorium geochemical data of southern Alaska river and lake sediment samples. (modified from Weaver 1983).

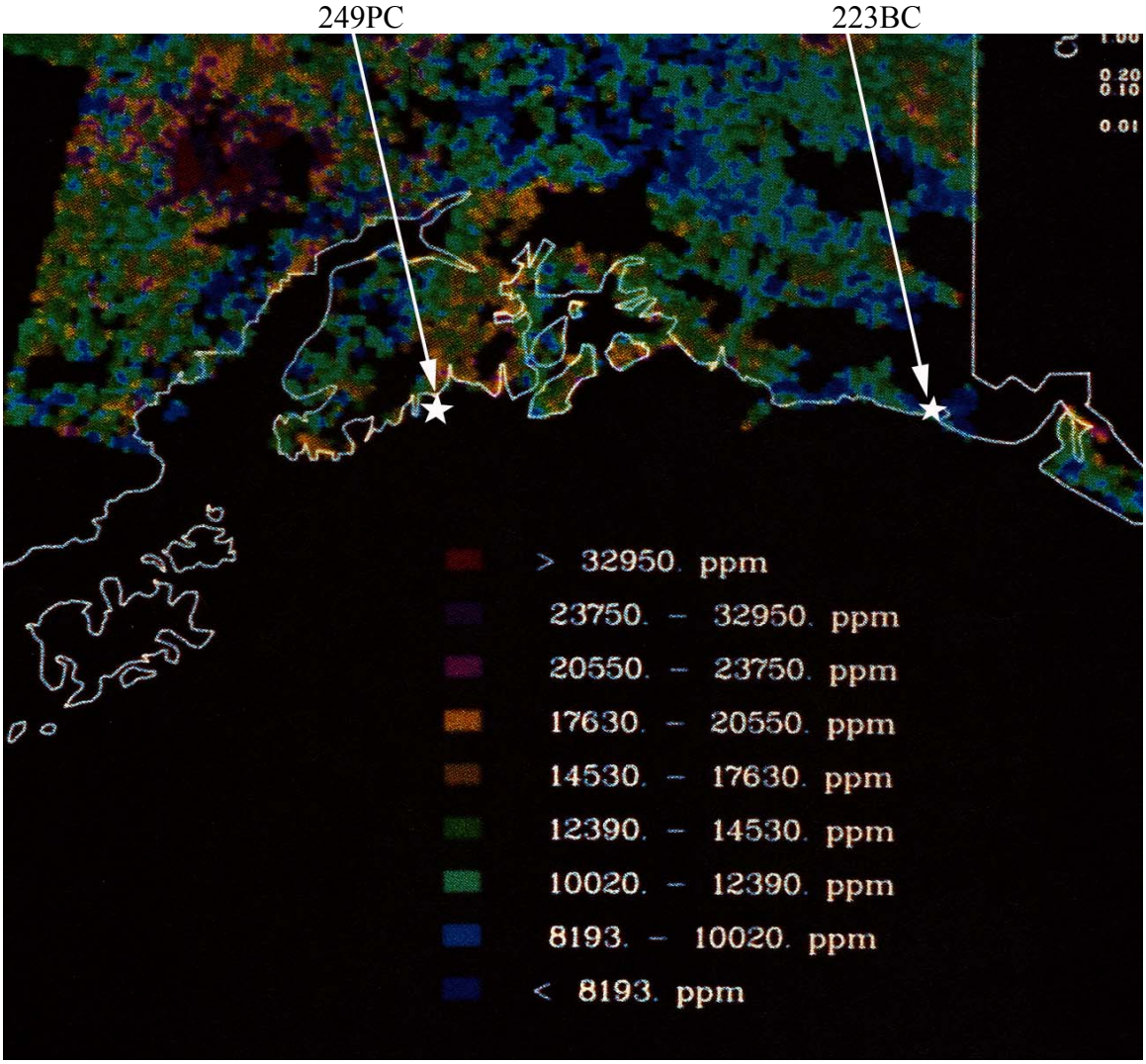

Figure 1-6. Published potassium geochemical data from southern Alaska lake and river sediment samples (modified from Weaver 1983).

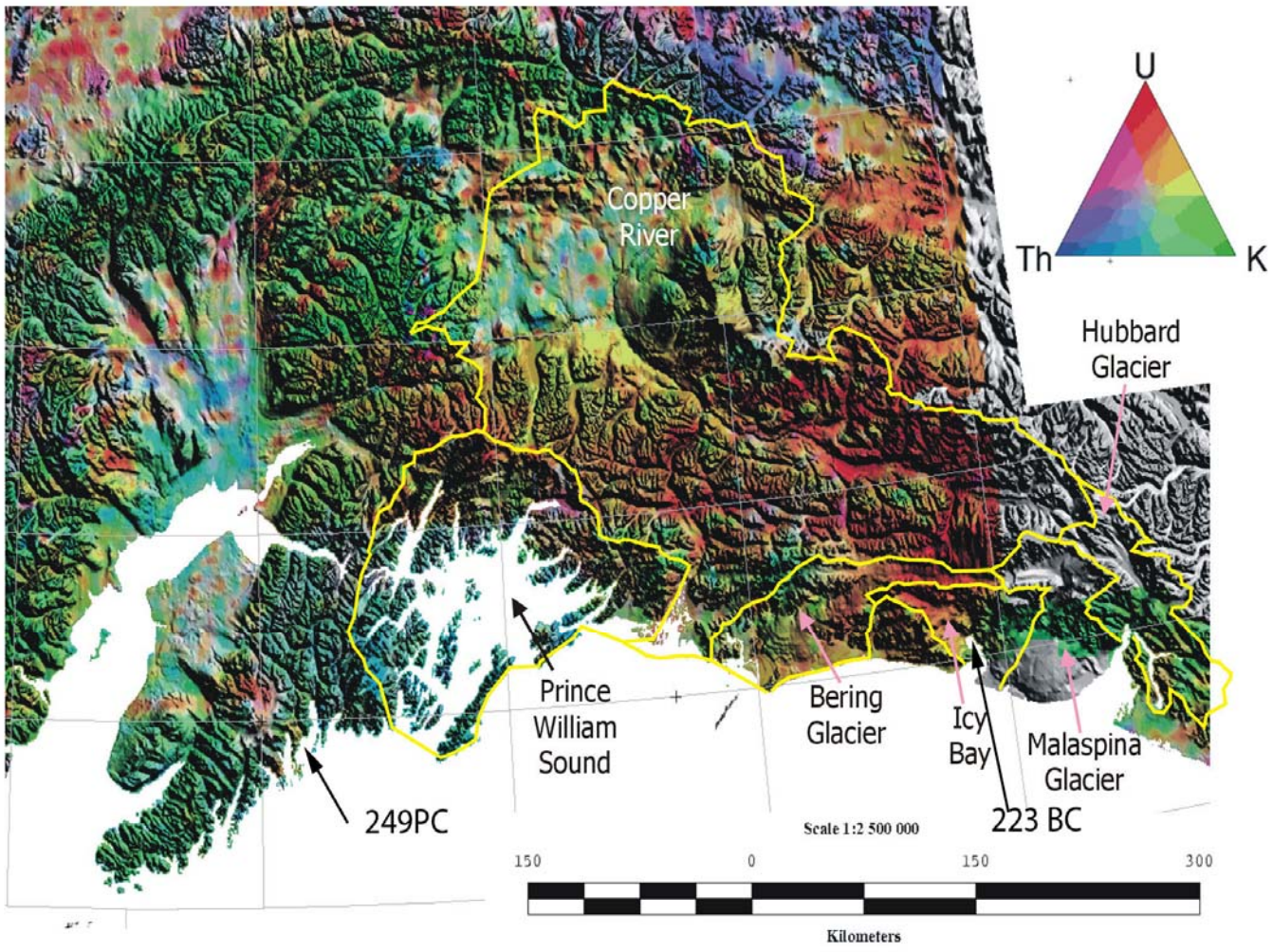

Figure 1-7. Aeroradiometric data of study area. Source area surrounding core 249PC shows elevated K and Th, while the environment near core 223BC shows elevated U and K. Drainage basins are outlined. (modified from Saltus et al. 1999).

CHAPTER 2
BACKGROUND

Regional Geology

Southern Alaska is a geologically complex area of accreted terranes representing relict Paleozoic, Mesozoic, and Cenozoic arc-trench systems, oceanic plateaus, and flysch basins (Figure 2-1). The landward side of the Pacific Plate boundary transform is a continental assemblage of five fault-bounded terranes that were accreted to the North American plate in the Mesozoic and Cenozoic. Additionally, the Yakutat terrane lies to the west of the Fairweather-Queen Charlotte fault and is currently being accreted to southern Alaska (Monger and Berg 1984; Dobson, O'Leary, and Veart 1998). Underthrusting and accretion of the Yakutat oceanic crust is apparent in a series of northeastward- to northward-dipping thrust faults. These include the Chugach-St. Elias, Contact, and Border Ranges fault systems (Plafker 1987; Mazzotti and Hyndman 2002).

The accretion of southern Alaska is summarized in steps by Hillhouse and Coe (1994). The core of Alaska was produced by the collision of the Wrangellia and Peninsular terranes with the Nixon Fork and Yukon-Tanana terranes during the interval 100 to 55 million years ago (Ma). This produced the crust of south-central Alaska, the ensuing Kula plate motion then likely provided the means to close the latitude gap between Wrangellia and the mainland. The counterclockwise rotation of southwestern Alaska most likely occurred 68 to 44 Ma as the latitude gap was closing. Volcanic complexes in the southern margin of the Chugach and Prince William terranes were added to Alaska after 55 Ma, carried by the Kula, then Pacific plates, respectively. Lastly, the ongoing accretion of the Yakutat microplate beginning around 30 Ma, has led to the uplift of the Chugach-St. Elias ranges bordering the GOA. It is currently amongst the most seismically and tectonically active regions in the world (Jaeger et al. 2001; Plafker,

Nockelberg, and Lull 1989). Interactions between the Pacific plate and overlying Yakutat microplate with the North American plate near the coastal margin have produced regions of high elevations and steep topography (Mazzotti and Hyndman 2002).

Icy Bay

Icy Bay has a complex geometry due to the recession of the Guyot Glacier, which occupied the bay until approximately 100 years ago. The Guyot, Yahtse, and Tyndall Glaciers have all been receding since 1904 (Jaeger and Nittrouer 1999). The recession has opened up four smaller fjords within the bay that had previously been filled with ice, and has left a moraine in the lower reaches of the bay. Sediment deposition within Icy Bay was studied extensively by Jaeger and Nittrouer (1999) who found that sediment from meltwater streams of Malaspina Glacier draining directly into the lower half of the bay greatly influence sediment input there. The drainage basin sits almost entirely among sediments of the Yakataga Formation (Figure 1-2). The Guyot Glacier is a tidewater glacier depositing directly into Icy Bay and sourcing the site for core 223BC.

Resurrection Bay

The Resurrection Bay area is characterized as a fjord coastline. Resurrection Bay is a deep glacially eroded segment of the GOA coastline. Broad alluvial fans were built by several creeks and the Resurrection River. Within a few hundred feet of shore steep slopes plunge hundreds of feet to the ocean bottom. Sediments in this fjord are derived from Bear Glacier, which overrides topography comprised almost entirely of rocks of the Valdez Group. The 249PC core site is located just outside the mouth of Resurrection Bay. (Figure 1-3)

Regional Glaciation

Glacial activity has been an intricate part of forming the topography throughout Alaska. It is described by Molnia and Hein (1982) as the single most important process controlling

sediment distribution in the GOA continental margin environment. The GOA area is bordered by high coastal mountains, which trap abundant moisture off the north Pacific. The abundance of glacial meltwater and rapid glacial motion lead to some of the highest erosion rates on the planet (10^5 tons km^2 y^{-1}, Hallet, Hunter, and Bogen 1996). Glaciation in the area is extensive and glaciers currently cover about 74,705 km^2 (5%) of Alaska, half of which occurs in the Kenai, Chugach, and St. Elias Mountains rimming the northern GOA (Calkin, Wiles, and Barclay 2001; Sauber and Molnia 2003). Most glaciers in southern Alaska are characterized as surging glaciers. The glaciers are more temperate compared to the Polar North Atlantic (Jaeger et al. 2001; Dobson et al. 1998).

Sedimentation

Sedimentary deposits are instrumental in recording the geologic and climatic evolution of modern environments. The history of uplift and glaciation in southern Alaska is recorded in sedimentary deposits throughout the Gulf region (Plafker 1987; Martin 1993). High basal debris loads (up to 1.5 m thick, Powell and Molnia 1989) and rapid glacial flow combine to produce large volumes of siliclastic glacimarine sediment. Sedimentation rates from the coastal mountains of southern Alaska have been estimated as the highest globally (Hallet et al. 1996; Hunter, Powell, and Lawson 1996; Powell and Molnia 1989). This rapid sedimentation is due to vigorous tectonic uplift, weakened bedrock, and heavy precipitation (Powell 1984; Hallet et al. 1996). Sediment delivery to the Gulf in southern Alaska is dominated by meltwater plumes in fjords and rivers emptying onto the shelf (Curran et al. 2003; Jaeger and Nittrouer, accepted; Sharma 1979). Many streams originate at the termini of active valley glaciers and carry sediment loads of up to >1g/l (Molnia and Hein 1982). Dominant controls on tidewater sedimentation (relevant to Icy Bay) are driven by seasonal fluctuations in meltwater discharge (Jaeger 2002).

Transport and Deposition

It is important to consider the history of the sediment to help constrain possible environmental effects. Generalized images of the two sites are presented. (Figs. 2-2, 2-3) The transport history of the particles analyzed from these two sites are relatively similar, because both are from a temperate fjord environment in the GOA. Both contain sediments characterized as rock flour, which were likely carried in meltwater from the glacier bed in a relatively dark, cold, vegetation-free environment (Anderson, Longacre, and Kraal 2003). Initial weathering of the source rock (Valdez Group for core 249PC, Yakataga Formation for core 223BC) preceded erosion. Heavy storms and high rates of precipitation (in the form of rain and snow) increase physical weathering in the Gulf environment, facilitating rapid erosion and transport of the sediment. Much of the sediment was incorporated into the respective glaciers which continually ground and crushed material as it moved down slope. Additional sediment was eroded from the valley walls and incorporated as the glacier moved. Sediment fluxes into temperate fjords such as this are generally controlled by meltwater discharge and calving (Jaeger and Nittrouer 1999). Glacial meltwater containing the rock flour was likely released as an englacial or subglacial jet and rose as a turbulent plume, which mixed with ambient water until it finally settled out (Powell and Molnia 1989; Syvitski 1988). In this environment, the coarsest material settles out quickly (often within 1 km of glacier terminus, Cowan, Powell, and Smith 1988) while the bulk of the fine sediment moves away from the fjords. Much of the fine-sized fraction is often carried in suspension onto the outer shelf (Sharma 1979).

Mean annual precipitation for the area near core 223BC is 100–200 cm higher than that of the area sourcing core 249PC (Figure 2-4). Rainfall amounts may affect sedimentation and transport processes including residence time, and have been shown to cause large variations in meltwater runoff from glaciers in southern Alaska (Cowan et al. 1988; Gustavson and Boothroyd

1982). The environment near Resurrection Bay likely has a slightly more complex depositional history relative to Icy Bay. The presence of a moraine and proglacial lake (Bear Lake) at Resurrection Bay between the Bear Glacier terminus and the Gulf may act as a trap for sediment. Seasonal precipitation and extremely high sediment discharge rates in the Gulf area make specific determination of residence times difficult, and beyond the scope of this project. The residence times within small drainage basins in the GOA environment are known to be short, as sediment is rapidly transported to the ocean (Jaeger et al. 1998).

Once material is deposited into the ocean, residence times of particles in the water column for both core sites are also estimated to be short based on observations of floc settling rates in other Alaskan tidewater fjords (Jaeger and Nittrouer 1999; Hill, Syvitski, Cowan, and Powell 1998). Re-suspension of bottom sediment allowing for increased residence in the water column is negligible because cores are taken in 145 m and 161 m water depth, and the wave orbital velocities necessary to re-suspend silt-sized bottom sediment only applies to depths < 40 m throughout the year and < 60 m for most of the year (Jaeger and Nittrouer, accepted).

Yakataga Formation

The Guyot Glacier is the source of the majority of sediments at core 223BC in Icy Bay. (Figure 1-2) Sediment sampled within the northern part of Icy Bay is derived principally from Upper Tertiary (Miocene to Pleistocene) rocks of the Yakataga Formation. The Yakataga Formation is located in the middle of an area of convergence and uplift on the GOA margin and is composed of interbedded terrestrial, marine, glacimarine, and glaciofluvial deposits that can locally exceed 5 km thickness (Bruns and Schwab 1983; Hamilton 1994). It represents rapid deposition of sediments consisting predominantly of sandstones, mudstones, siltstones, shale and conglomerates (Mazzotti and Hyndman 2002; Sauber and Molnia 2003). Glaciation recorded by the Yakataga Formation is attributed to orogenic uplift and increased precipitation resulting from

the collision of the Yakutat terrane with the North American plate (Turner 1992). Clay mineral suites (illite, kaolinite, chlorite and smectite) within it are relatively similar to those of the modern shelf (Molnia and Hein 1982). Accumulation of recycled sedimentary material comprising the Yakataga Formation is estimated to have begun near mid-Miocene.

Valdez Group

The other study site is in the Resurrection Bay area of the GOA. (Figure 1-3) The sediments here are supplied from the Bear Glacier, which sits entirely with rocks of the Valdez Group of the Chugach terrane. This group, a series of arc-derived slope and trench clastic deposits that comprise the vast majority of the outer Kenai Peninsula, is part of a flysch sequence which forms the southern part of the Chugach terrane (Ward, Moslow, and Finkelstein1987; Nockleberg et al. 1994). The sedimentary rocks that compose it have been derived largely from a Phanerozoic continental margin arc complex characterized by igneous rocks (Plafker, Moore, and Winkler 1994). Latest Cretaceous to early Paleocene arc-continent collision resulted in off-scraping and accretion to the continental margin of the flysch, mixed flysch and basaltic tuff, and basalt which principally comprise the Valdez Group (Lang Farmer et al. 1993; Lull and Plafker 1989). Precambrian crustal material is present, possibly derived from late Proterozoic or older metasedimentary and metaigneous rocks (Lang Farmer et al. 1993).

Mineralogy

Most major glacimarine depositional systems are siliclastic (Powell and Molnia 1989). The clay mineral content is controlled principally by 1) climate and relief, 2) type (mineralogy) of weathered source material, 3) chemical composition of weathering solutions, and 4) later diagenesis within the depositional environment (Brownlow 1996; Schnyder et al. 2005). The most common clay minerals in soils, sediments, and sedimentary rocks are kaolinite, illite, smectite clays, and chlorite clays (Brownlow 1996). The average clay-sized (<2 μm) sediment

in southern Alaska (Molnia and Hein 1982) is predominantly kaolinite + chlorite (61 %), intermediate illite (37 %), and low smectite (2 %), representing an immature sediment characterized by rapid mechanical weathering and little chemical alteration. Analysis of the non-clay mineralogy of the clay-sized fraction by Molnia and Hein (1982) identified the presence of accessory minerals which include but aren't limited to quartz, feldspar, amphibole, and calcite.

Radioisotopes

Gamma-ray measurements are non-destructive, efficient methods of formation evaluation and can be a valuable tool in both the environmental and engineering fields (Nir-El 1997, Ayres and Theilen 2001). A study by Schnyder et al. (2005) notes the use of radioisotopes in a variety of geological applications, including sequence stratigraphy (van Wagoner et al. 1990), reservoir characterization, diagenesis and mineral characterization (Hurst 1990), and source-rock evaluation. Gamma-ray measurements detect variations in natural radioactivity originating from changes in concentrations of the trace elements uranium (U) and thorium (Th), as well as the more common rock-forming element potassium (K). The abundance and half-lives of U, Th, and K (Table 2-1) make these three elements the dominant sources of gamma-rays detected, and thus the most important natural radionuclides for many geological studies (Ruffell and Worden 1999; Ayres and Theilen 2001). Decay of the parent radioisotope ^{238}U gives rise to one of the uranium decay series. The isotopic composition and concentrations of uranium, thorium (and their associated daughter products) and potassium have previously been used as a dating and fingerprinting tool (Blum 1995; Harlavan and Erel 2002; Blum and Erel 1997). Particularly for the purposes of this thesis, it is important to note that clay mineralogy is controlled primarily by weathered source rock, climate, transport, and deposition, which then influence the spectral gamma-ray (SGR) response of the sediments (Schnyder et al. 2005).

Uranium and thorium have many host minerals in sedimentary rocks including clays, feldspars, phosphates, and zircons (McLennan et al. 2003; Weltje and Eynatten 2004). Thorium, which is widely distributed in igneous rocks, is considered at least partially insoluble and thus is often concentrated in sediments during weathering (Schnyder et al. 2005). Both uranium and thorium tend to be highly concentrated in trace accessory minerals such as zircon, monazite, apatite, and sphene (Blum and Erel 1997). Potassium is abundant in sediments and is concentrated particularly in alkali feldspar and biotite, it is considered soluble in aqueous solutions (White et al. 1999; Ruffell and Worden 1999). The amount of ^{238}U in natural uranium accounts for 99.27 % of total uranium, and ^{232}Th accounts for almost all (assumed 100%) of total thorium. ^{40}K compromises an average of 0.0118% of total potassium, which is actually very significant because potassium is one of the ten most surface-abundant elements on earth (Irwin, VanMouwerik, Stevens, Seese, and Basham 1997; Hutchison and Hutchison 1997).

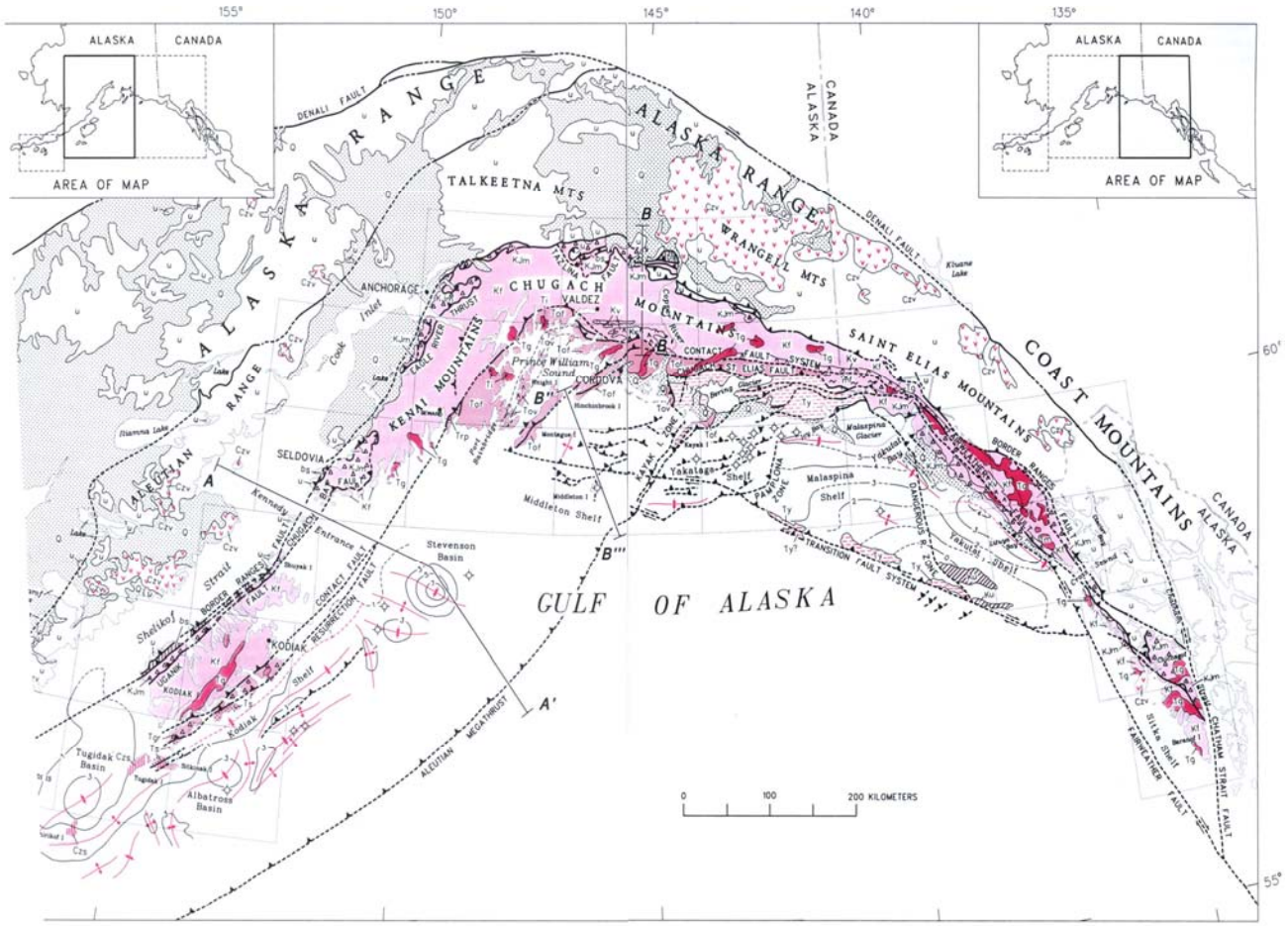

Figure 2-1. Structural formations on the southern Alaska margin (modified from Plafker et al. 1994).

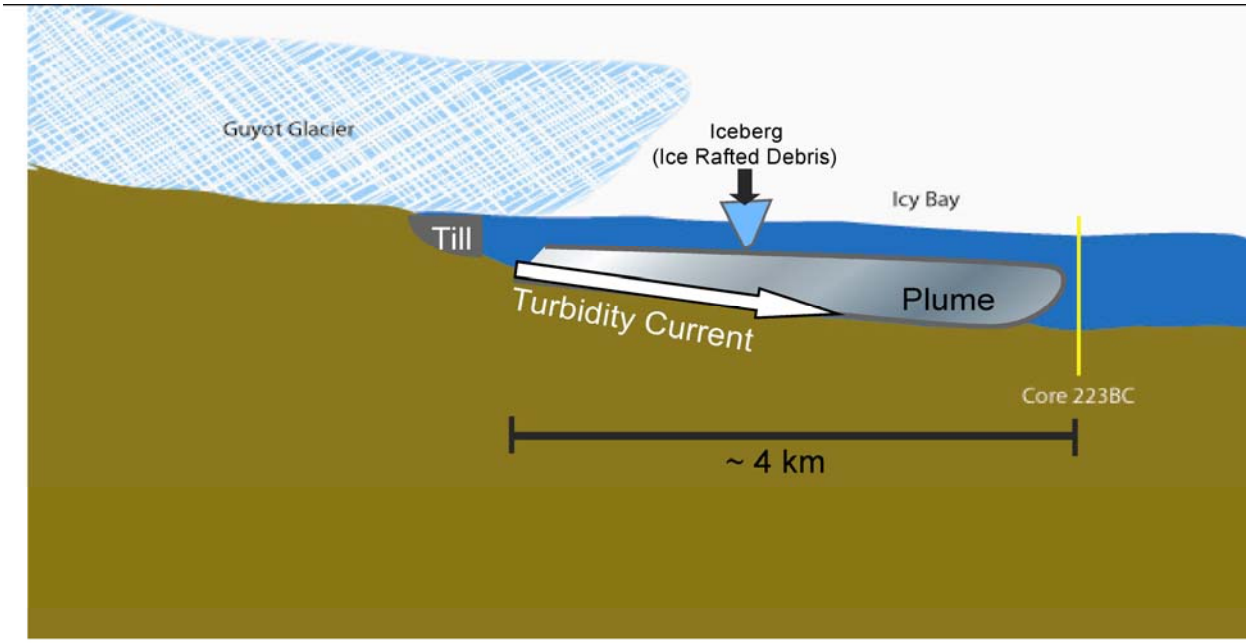

Figure 2-2. Generalized sketch of the cross section near core 223BC.

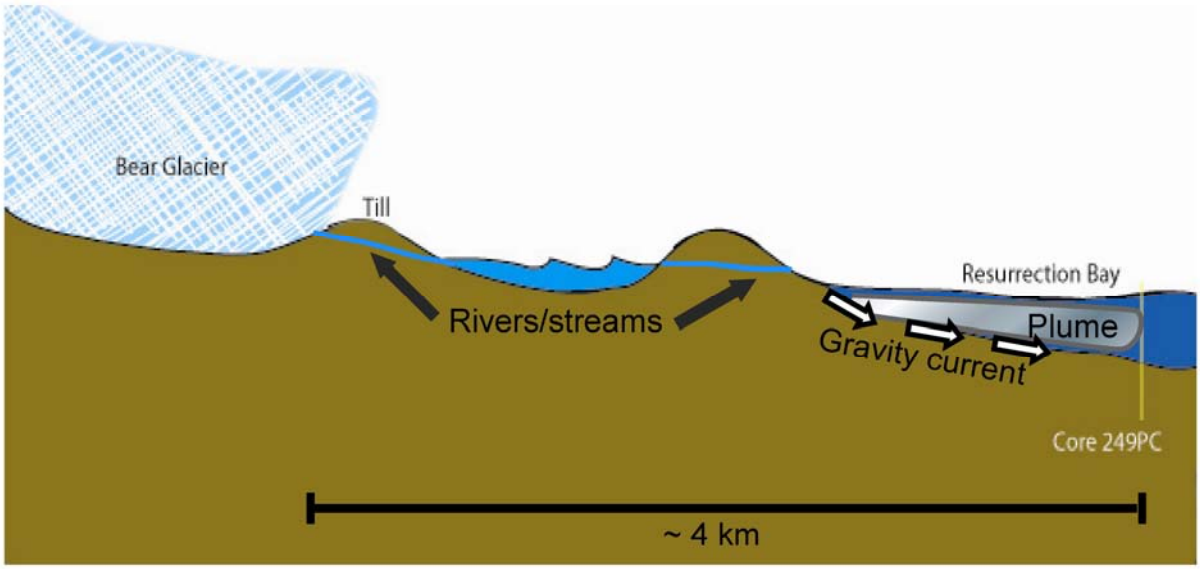

Figure 2-3. Generalized sketch of the cross section surrounding core 249PC.

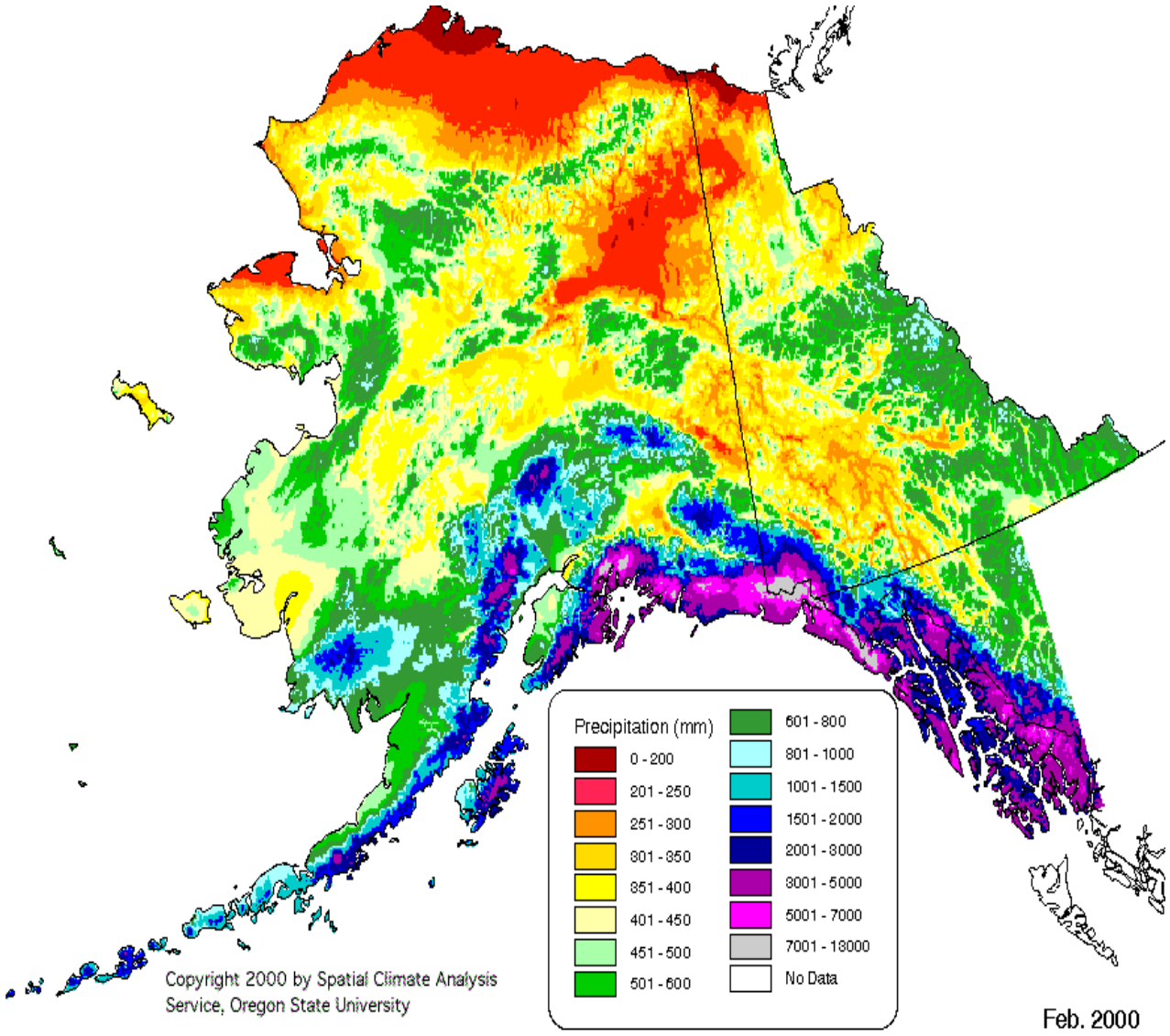

Figure 2-4. Mean annual precipitation for the state of Alaska. Note that the area surrounding Resurrection Bay (core 249PC) has a range of 1501-5000 mm/yr while the area surrounding Icy Bay (core 223BC) shows levels from 3001-13000 mm/yr. (reprinted with permission from Spacial Climate Analysis Service, Oregon State University 2000).

Table 2-1. Half lives and average abundances of relevant radioisotopes

Radioisotope	^{40}K	^{232}Th	^{238}U
Half-life (billion years)	1.277	14.05	4.468
Upper continental crust			
Elemental abundance (ppm)	28000	10.7	2.8
Activity (Bq/kg)	870	43	35
Activity (nCi/kg)	23	1.2	0.9
Activity (kCi/km3)	66	3.3	2.6
Oceans			
Elemental concentration (mg/liter)	399	$1x10^{-7}$	0.0032
Activity (Bq/liter)	12	$4x10^{-7}$	0.04
Activity (nCi/liter)	0.33	$1x10^{-8}$	0.0011
Ocean sediments			
Elemental abundance (ppm)	17000	5	1
Activity (Bq/kg)	500	20	12
Activity (nCi/kg)	14	0.5	0.3

CHAPTER 3
METHODS

Sampling

Piston core 249PC and box core 223BC were chosen for this study based on the differing lithologies of their sediment sources. Also considered was the similar proximity to glacial termini (~4 km), with similar water depths (~150 m). Using glacier-proximal core sites allows for the assumption that post-depositional physical and chemical alteration is minimal (e.g., slumping, turbidity flows, biological activity). The proximal location of these cores also increases the likelihood that these sediments accurately represent source material, relative to cores taken further out onto the shelf. Core samples used in this study were collected on the *R/V Alpha Helix* during June and July 1995.

Core location is important because it is necessary to minimize influences from other sources. Core 223 was taken in 145 m depth water approximately 4 km from the ice front in Icy Bay, a fjord located on the eastern side of the southern Alaska GOA margin. Core 249PC was taken close to Resurrection Bay in 161 m water depth approximately 4 km from the coast, near Bear Glacier. These locations allow for minimal influence of material associated with a source other than the Yakataga Formation for core 223BC or the Valdez Group for core 249PC. (Figs 1-2, 1-3)

Core 249PC was separated into 10 cm intervals (0–10 cm, 11–20 cm, and 21–30 cm) at the University of Florida. During sampling a box core was subsampled with a 15 cm-diameter, 50 cm-long subcore, creating core 223BC. Core 223BC had been previously segmented into 1 cm intervals and placed in whirlpak bags. Intervals 11–12 cm, 15–16 cm, 20–21cm, and 31–32 cm were chosen based on availability and similarity to depths of core 249PC. The core 223BC site experiences higher sedimentation rates (>100 cm y^{-1}; Jaeger and Nittrouer 1999) than those at the

site of core 249PC (~ 1 cm y^{-1}; Jaeger et al. 1998). Sediment depositional rates at the site of core 249PC in Resurrection Bay have not been as tightly constrained as those in Icy Bay but can assumed based on observations from surrounding areas (Jaeger et al. 1998). The sediments within core 249PC near Resurrection Bay, therefore, represent a longer time period than sediment retrieved in the Icy Bay core.

Radioisotope Evaluation

Radioactivity measurements of ^{232}Th, ^{238}U and ^{40}K were performed on dried and powdered sediment. These samples were counted on a Canberra UltraLow Background Planar-Style germanium detector at the University of Florida. The amount of sample used varied by availability, but averaged 15 g for core 249PC and 12 g for core 223BC. Count times ranged from 80,240 to 160,993 seconds but averaged 90,245 (about 25 hours), in order to accurately measure activity and minimize error. Raw gamma spectroscopy data was processed by analyzing photopeaks generated using Gamma Genie software.

Background levels were determined by running an empty sample jar and subtracting the background value for each region of interest in the sample spectra. Efficiency was determined by counting a sample (NIST standard) with known activity and comparing it with the amount detected on the instrument at the University of Florida. Self-absorption correction factor calculations were made for radioisotopes with gamma decay energies of less than 200 keV, which for this study affects only measurements of ^{234}Th (related to ^{238}U activity) at the 63 keV photopeak. This technique involves direct gamma transmission measurements on sample and efficiency calibration standards (see Cutshall, Larsen, and Olsen 1983 for further explanation).

Radionuclide activity determinations were made by converting the raw data from counts per minute (cpm) to decays per minute (dpm), then dividing by sample weight. The standard form of conversion from activity (dpm/g) to concentration (ppm) is a process requiring the

conversion of activity to atom quantity. Concentration determinations for these analyses were done using efficiencies previously established from the Buffalo River and an estuary (with known concentrations) for the radioisotope of interest. The cpm value is determined by dividing the net peak area by counting time. The 63 keV photopeak corresponding to ^{234}Th activity was examined to determine ^{238}U activity (Figures 3-1, 3-2). A similar technique was used to obtain ^{232}Th activity by measuring photopeaks associated with activity of the daughter ^{228}Ac (half life = 6.13 d). Though no specific measurement was made, the daughter is assumed to be in secular equilibrium with ^{232}Th (half life = 1.4×10^{10} yr), since it has a significantly shorter half life and we assume minimal loss of ^{228}Ra. For a more accurate measurement, weighted averages of two peaks associated with ^{228}Ac (a high energy gamma-ray at 911 keV as well as the 338 keV ray) were used. Multiple photopeaks are often averaged for more accurate ^{228}Ac measurements (Nir-El 1997).

Secular equilibrium is the condition in which the rate of decay of the daughter is equal to that of the parent, and most commonly occurs when the daughter has a significantly shorter half life than the parent. For ^{232}Th and ^{238}U, the half lives are significantly longer than those of their daughters (Table 2-1), satisfying necessary conditions to enable this type of analysis (Faure 1986). ^{40}K was measured directly at the 1461 keV photopeak.

Precision was determined by running two random samples on three separate occasions and determining the mean deviation from the mean. Due to the small data set and associated scatter, it is more appropriate to use this deviation as opposed to a standard deviation in order to better represent error. This procedure established errors for the radionuclides (^{238}U ±0.7 ppm, ^{232}Th ±0.4 ppm, and ^{40}K ±0.1 %). The largest deviation for each particular element was selected. (Table 3-1)

Grain Size Separation

Grain size separation in preparation for radioisotopic analysis was done at the University of Florida using sieve and Sedigraph analyses (Lewis and McConchie 1994; Syvitski 1991). Dry sediment samples weighing approximately 10 g (core 249PC) or 2.5 g (core 223BC) were homogenized then put into 120 milliliter (ml) glass jars and soaked in a 0.05 % sodium metaphosphate ($Na(PO_4)_5$) solution overnight in order to help disaggregate particles. Those showing signs of flocculation were soaked an additional day in 1.0 % $Na(PO_4)_5$ solution. Samples were placed in an ultrasonic bath for a minimum of 10 minutes before being wet-sieved through a 63 μm sieve in order to isolate the sand-sized fraction which was then dried and weighed. The silt fraction was isolated by adding de-ionized water and diluting the clay/silt mixture to improve settling velocity. The mixture of approximately 500 ml was then agitated and allowed to settle in a water column based on the application of Stoke's Law (in accordance with Lewis and McConchie 1994). After the designated time, the remaining liquid was siphoned leaving only the silt fraction. The clay fraction was separated by siphoning followed by either centrifugation or drying in a low-temperature (< 60º F) oven. Random samples were selected to run on the Sedigraph as a check to determine if any remaining silt was left in suspension, and was found to be negligible (<1%).

Radioisotopic activity is normalized to the mass of the counted sample (i.e., dpm/g). The sand-sized (>63 μm) fraction was separated and weighed, then divided by the original mass to get percent sand. The fine-sized fraction was then mixed with 0.05 % $Na(PO_4)_5$ and run on a Sedigraph 5100 analyzer to determine percent silt and percent clay (error was found to be less than 0.6 % in each interval). Additionally, all intervals were normalized according to mass percent clay to eliminate biases associated with increased mass due to increased sand content (Table 3-2).

Mineralogy

Microscopic Evaluation

Mineralogy of the sand-sized fraction was determined in part by analysis of smear slides constructed using techniques of the I.O.D.P. and Flemings et al. (2006). Slides were created by sprinkling a small amount of homogenized sediment on a 2.5 cm x 7.5 cm glass slide and dispersing it over the slide with a drop of deionized water. The sample was then dried on a hot plate at a low temperature for approximately 5 minutes. A drop of Norland optical adhesive and a 2.5 cm x 2.5 cm cover glass were placed over the sample. The slide was then put under an ultraviolet light to dry and set. Point count data was done on a Nikon petrographic microscope with an integrated automatic point counter. Slides were analyzed at 1000 counts per slide spaced at approximately 1 mm.

X-Ray Diffraction

Bulk mineral analysis of homogenized sediment was prepared for conventional powder mount x-ray diffraction (XRD) in accordance with Lewis and McConchie (1994) and done at the University of Florida. Approximately 2 g of sediment was taken from a central interval in each core (11–20 cm for core 249PC, 15–16 cm for core 223BC).

Table 3-1. Precision data for associated each radionuclide measured. The largest mean deviation about the mean measured was chosen to obtain greatest accuracy.

	U (ppm)	Th (ppm)	K (%)
run 1	3.5	5.9	1.5
run 2	2.8	5.4	1.6
run 3	2.1	6.6	1.5
Average	2.8	5.9	1.5
mean deviation	0.7	0.4	0.04
run 1	3.2	3.7	2.1
run 2	3.2	3.2	2.4
run 3	3.7	2.7	0.1
Average	3.4	3.2	2.2
mean deviation	0.2	0.3	0.1

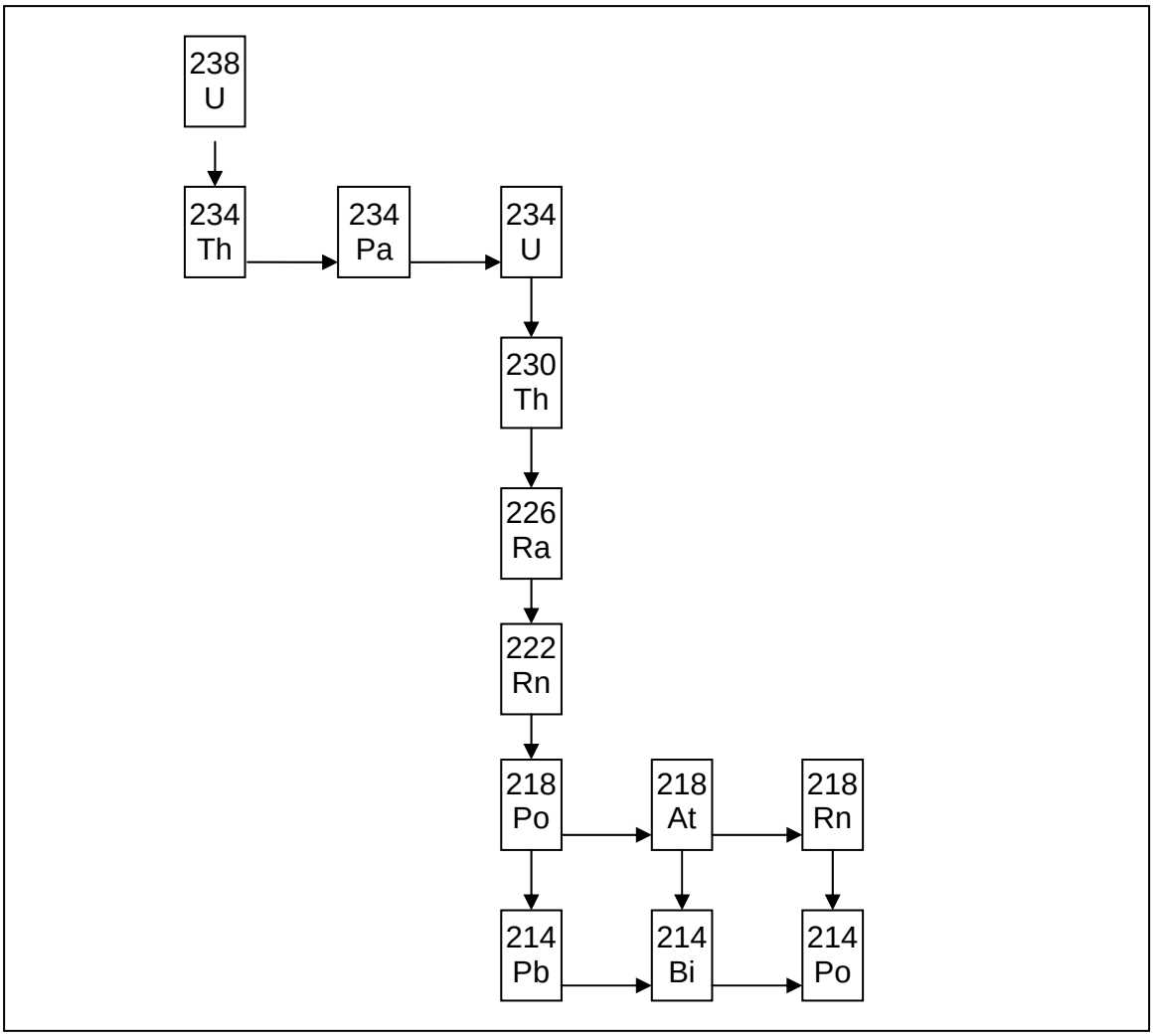

Figure 3-1. Decay series of the ^{238}U radioisotope relevant to this study.

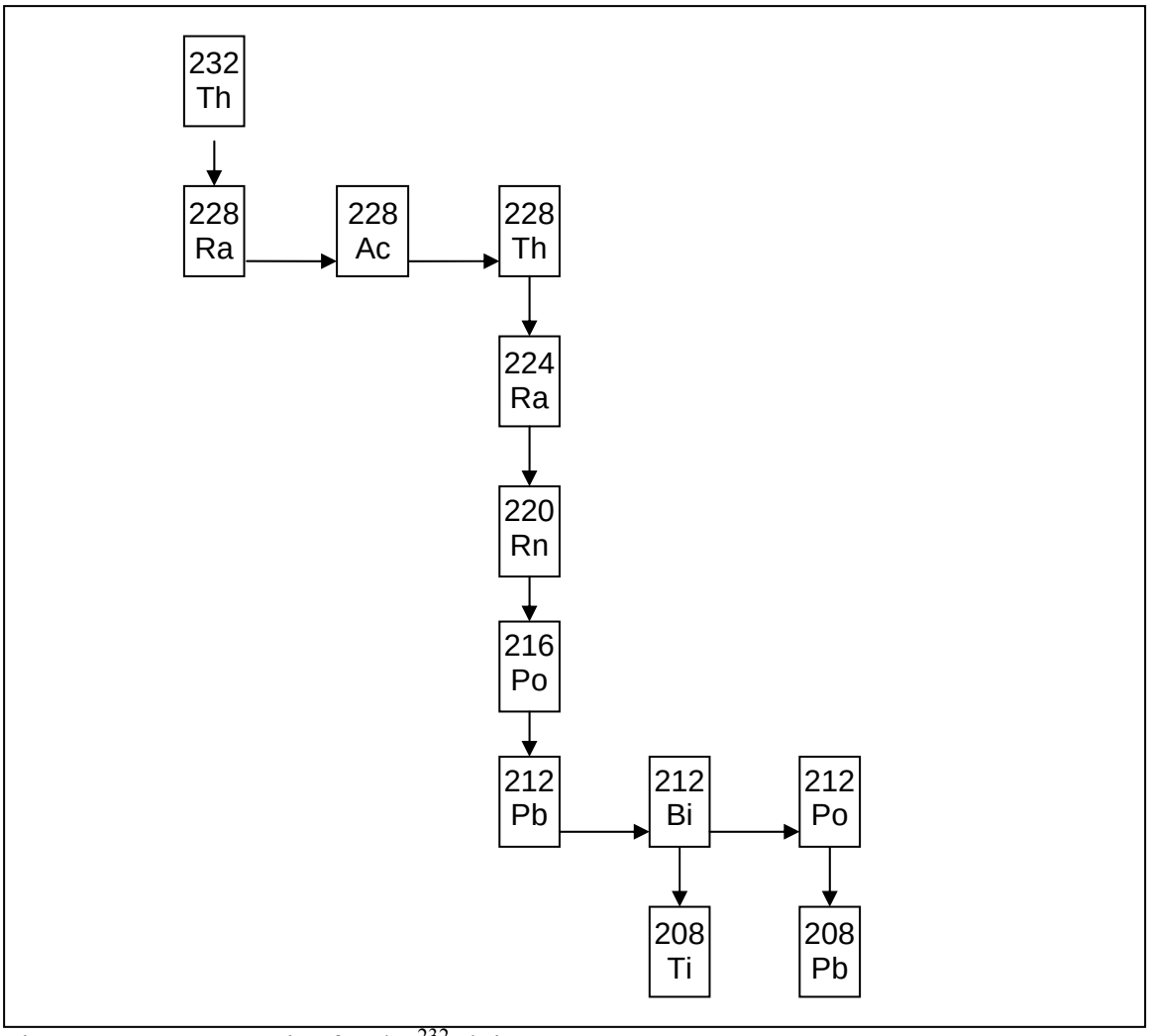

Figure 3-2. Decay series for the ^{232}Th isotope.

Table 3-2. Elemental concentration data normalized to clay percent. The measured (original) concentrations are also listed for comparison. Only bulk sample measurements are presented.

Concentrations (normalized to clay)					Original Concentrations		
	DEPTH	U (ppm)	Th (ppm)	K (%)	U (ppm)	Th (ppm)	K (%)
CORE 249PC							
249 PCa	0–10 cm	6.4	4.7	3.5	4.5	3.1	2.5
249 PCb	0–10 cm	5.6	8.1	3.2	4.0	5.8	2.3
249 PCc	0–10 cm	6.0	7.0	3.4	4.2	5.0	2.4
249 PCa	11–20 cm	5.6	6.1	3.4	4.0	4.4	2.4
249 PCb	11–20 cm	6.1	5.9	3.3	4.3	4.3	2.4
249 PCc	11–20 cm	6.4	7.2	3.4	4.6	5.2	2.4
249 PCa	21–30 cm	7.2	9.2	3.9	4.1	5.3	2.2
249 PCb	21–30 cm	8.8	10.0	4.0	5.0	5.8	2.3
249 PCc	21–30 cm	7.2	11.4	4.0	4.1	6.6	2.3
CORE 223BC							
223 BC	11–12 cm	1.6	3.7	2.4	3.7	4.1	2.0
223 BC	15–16 cm	4.8	5.0	2.6	3.2	3.4	1.8
223 BC	20–21 cm	4.1	0.8	0.4	2.4	0.6	0.3
223 BC	31–32 cm	2.7	3.2	1.4	1.7	2.1	0.9

CHAPTER 4
RESULTS

Radioisotopic Analysis

Core 249PC exhibited comparable concentrations throughout the core for each element (Table 4-1, Figs. 4-1 through 4-6). The uranium concentration (averaged from replicates of each interval) in core 249PC ranged from 4.2 ppm to 4.4 ppm, whereas in core 223BC it ranged from 1.7 ppm to 3.7 ppm. Thorium concentration in core 249PC ranged from 4.6 ppm to 5.9 ppm as opposed to the core 223BC range of 0.6 ppm to 4.1 ppm. The potassium percentage also showed more consistency in core 249PC, ranging from 2.3 % to 2.4 %, whereas core 223BC ranged from 0.3 % to 2.0 %. Although core 223BC did show increased variability in ranges of element concentrations, there remained a consistent overall decrease of activity with depth. Uranium showed a relatively linear trend of decreasing concentration with increased depth. The thorium concentration in core 223BC decreases in general, the exception being interval 20–21 cm, which exhibited low thorium and potassium. This interval was different from all other intervals in that it exhibited a significantly higher uranium (2.4 ppm) concentration relative to extremely low thorium (0.6 ppm) and potassium (0.3 %).

Detailed concentration data on separated size fractions is shown in Table 4-2. There is little evidence that elemental thorium concentrations are enhanced within a particular size fraction for either core, it is at times highest in each of the three size fractions. The concentration of uranium is not associated with the sand-sized fraction. It is always highest in either the clay- or silt-sized fraction, but varies between the two. For potassium there is a distinct correlation of concentration and grain size throughout both cores. The clay (<2 μm) fraction contains the highest concentration relative to silt and sand at every interval. The potassium percentage is also lowest in the sand fraction at every interval. Each element is plotted against clay percent. (Figs.

4-7 through 4-9) Concentration data once normalized to clay, which assumes 100 percent clay-sized material, is shown compared to bulk concentration. (Table 3-2)

Mineralogy and Physical Properties

Core 249PC

Mineralogic data for all three intervals of core 249PC showed a higher abundance of rock fragments (ranging from 78-86%) when compared to core 223BC (61-68%). (Figs. 4-10 through 4-14) There was also an appreciable amount of quartz in core 249PC (9-11%) at all three intervals. Biotite and amphibole were the next most common minerals. Accessory minerals compromising less than 1% of the sample include, but are not limited to, pyroxene, garnet, biogenic material, opaque minerals (hematite, ilmenite), and glass (Figs. 4-15 through 4-24).

Core 223BC

Due to the limited amount of sand available for core 223BC intervals 11–12 cm and 31–32 cm, no smear slides were made. Point count data for core 223BC on intervals 20–21 cm and 15–16 cm (the only two slides for core 223BC) show an overall decrease in rock fragments and increase in quartz [relative to 249PC]. (Figs. 4-13, 4-14) Quartz abundances for core 223BC (22 % and 27 %) were at least twice that of those observed in core 249PC. The core 223BC interval containing fewer rock fragments (15–16 cm) had a corresponding increase in quartz fragments (27%). Biotite occurrence is at 4% for both intervals, while amphibole and accessory minerals show a slight (1% to 2%) increase in the 15–16 cm segment.

Relative to core 249PC, core 223BC contains more quartz and fewer rock fragments, with a more angular shape. Mineralogy of the fine-sized fraction is very similar between cores (Figure 4-25). From XRD analysis, the most significant peak corresponds to quartz at 26.67 (at $2\theta_{Cu}$), and is noted again at secondary peaks (e.g., 50.21). The peaks corresponding to illite, chlorite, and kaolinite are all elevated in core 249PC relative to core 223BC. This is expected

due to the higher percentage of clay in core 249PC relative to 223BC. Core 223BC contains one additional mineral (likely a feldspar) which is not present at core 249PC.

Grain Size

Grain size separation shows an average of ~66% clay, ~26% silt, and ~8% sand for core 249PC from 0-30 cm, with specific intervals ranging from 57 % to 71 % clay. (Table 4-3) There is an increase in silt with depth (22% to 31%), and an overall increase in sand (8% to 12%). The core 249PC interval 21–30 cm shows a significant decrease in percent clay and increase in percent sand (57% clay, 12% sand).

Grain size averages for core 223BC are 62% clay, 33% silt, and 3% sand, with clay ranging from 58 % to 67 %. There is an overall slight decrease in percent clay with depth (67% to 61%). Contrastingly, there is an overall slight increase of both percent silt (31% to 38%) and percent sand (2% to 6%) with depth. The exceptions are interval 15–16 cm which exhibits a slight decrease in percent silt from the interval above it, and interval 31–32 cm which exhibits distinctly low sand content.

Table 4-1. Radionuclide concentration data and associated error of each bulk sample within each interval.

	^{238}U (ppm)	error	^{232}Th (ppm)	Error	^{40}K (%)	error
249PC						
0–10cm	4.2	±0.7	4.6	±0.4	2.4	±0.1
11–21cm	4.3	±0.7	4.7	±0.4	2.4	±0.1
21–30cm	4.4	±0.7	5.9	±0.4	2.3	±0.1
223BC1						
11–12cm	3.7	±0.7	4.1	±0.4	2	±0.1
15–16cm	3.2	±0.7	3.4	±0.4	1.8	±0.1
20–21cm	2.4	±0.7	0.6	±0.4	0.3	±0.1
31–32cm	1.7	±0.7	2.1	±0.4	0.9	±0.1

Note: For core 249PC, the three bulk samples were averaged

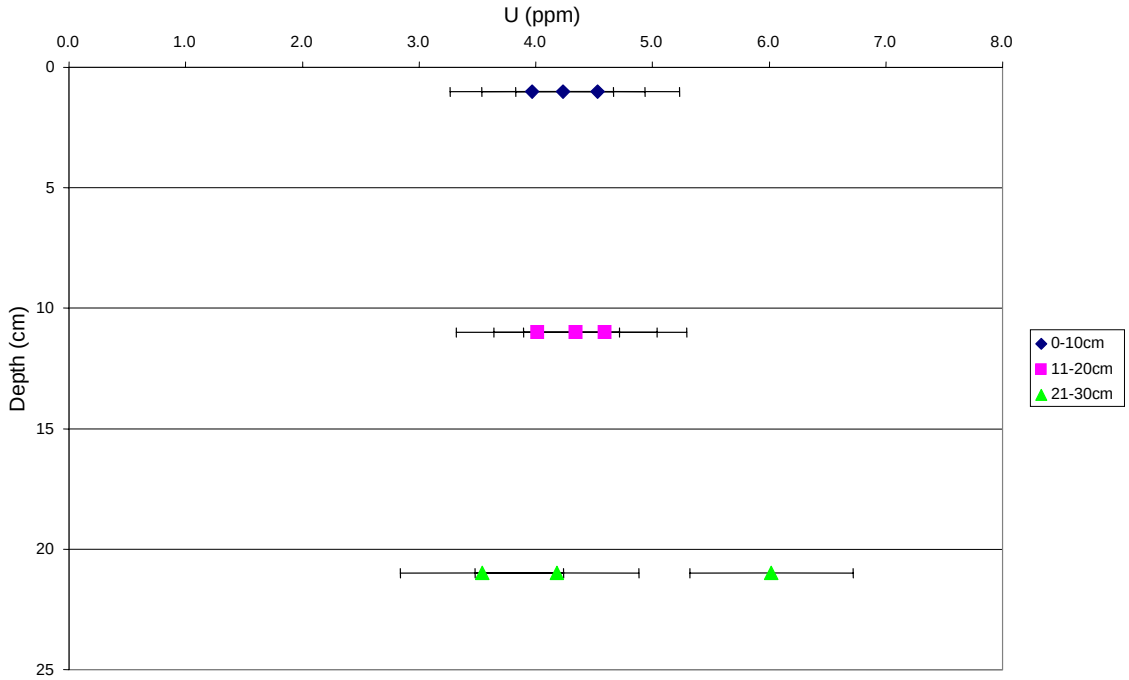

Figure 4-1. Concentration of uranium with depth in core 249PC.

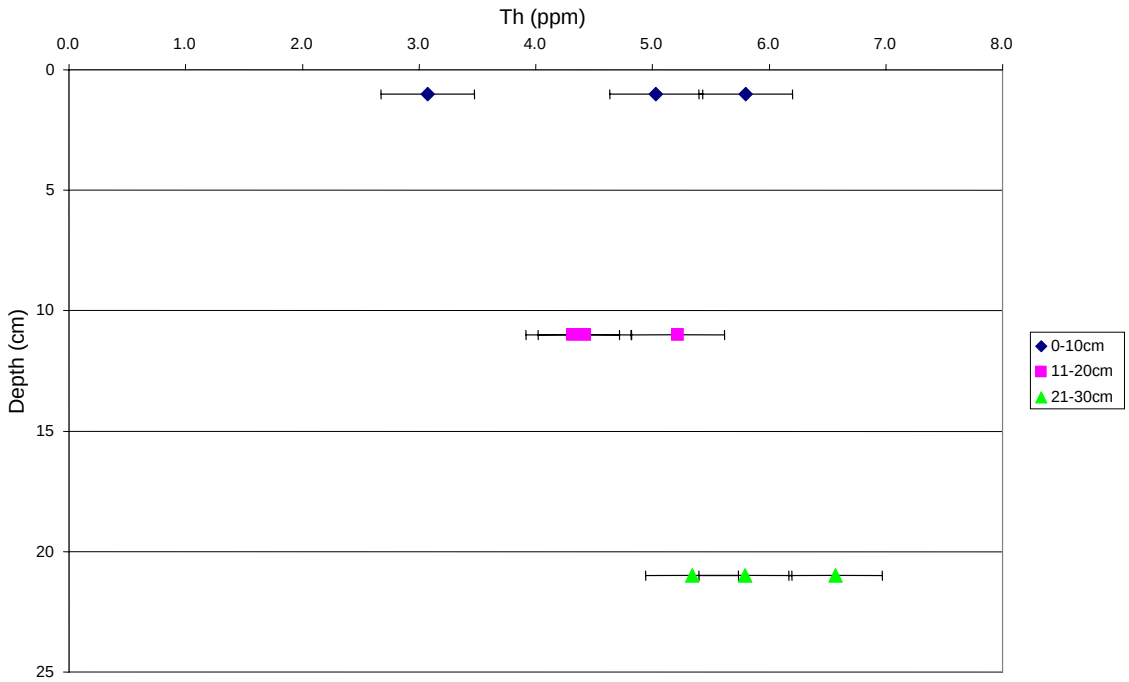

Figure 4-2. Concentration of thorium with depth in core 249PC.

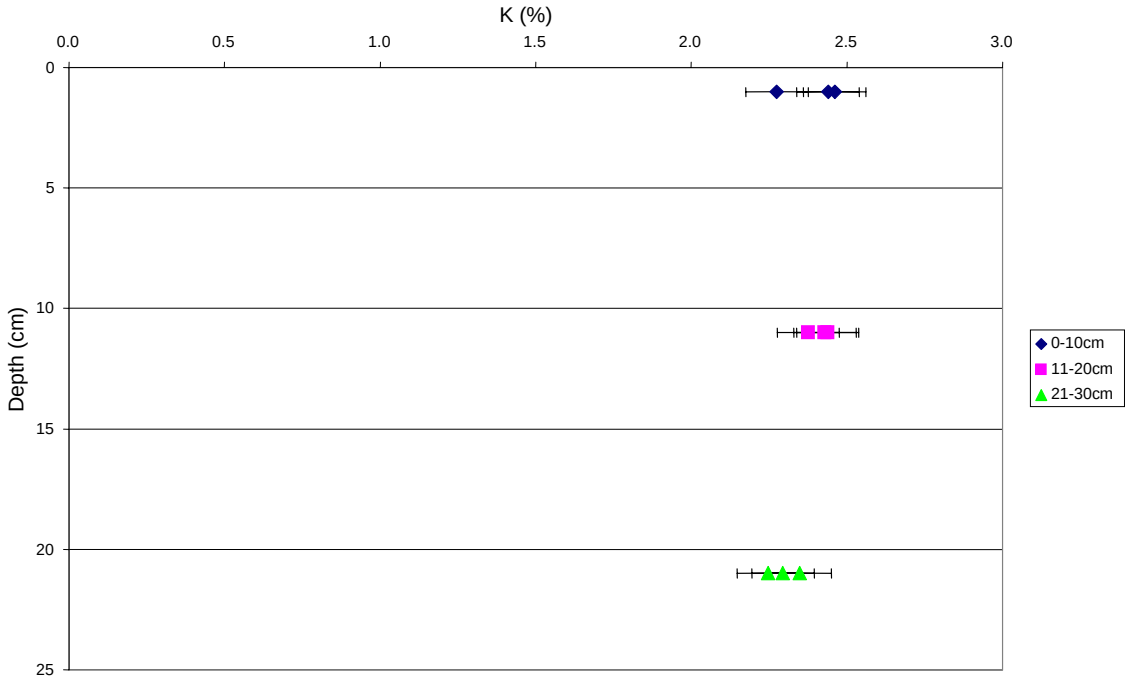

Figure 4-3. Radioisotopic concentration of potassium with depth in core 249PC.

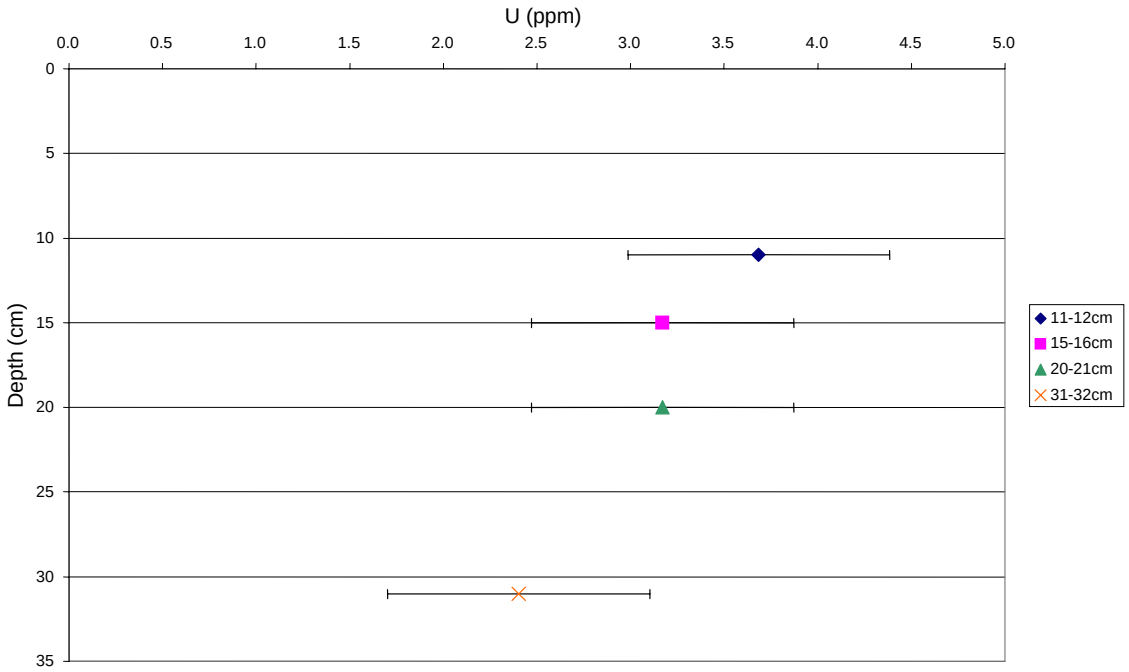

Figure 4-4. Concentration of uranium with depth in core 223BC.

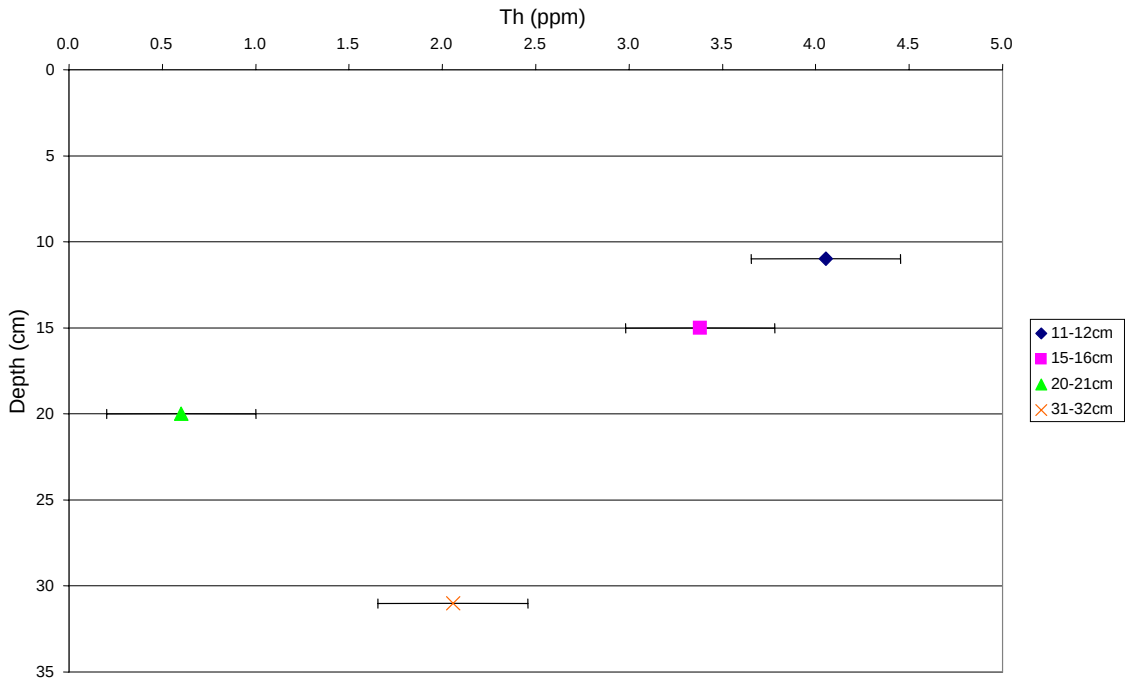

Figure 4-5. Concentration of thorium with depth in core 223BC.

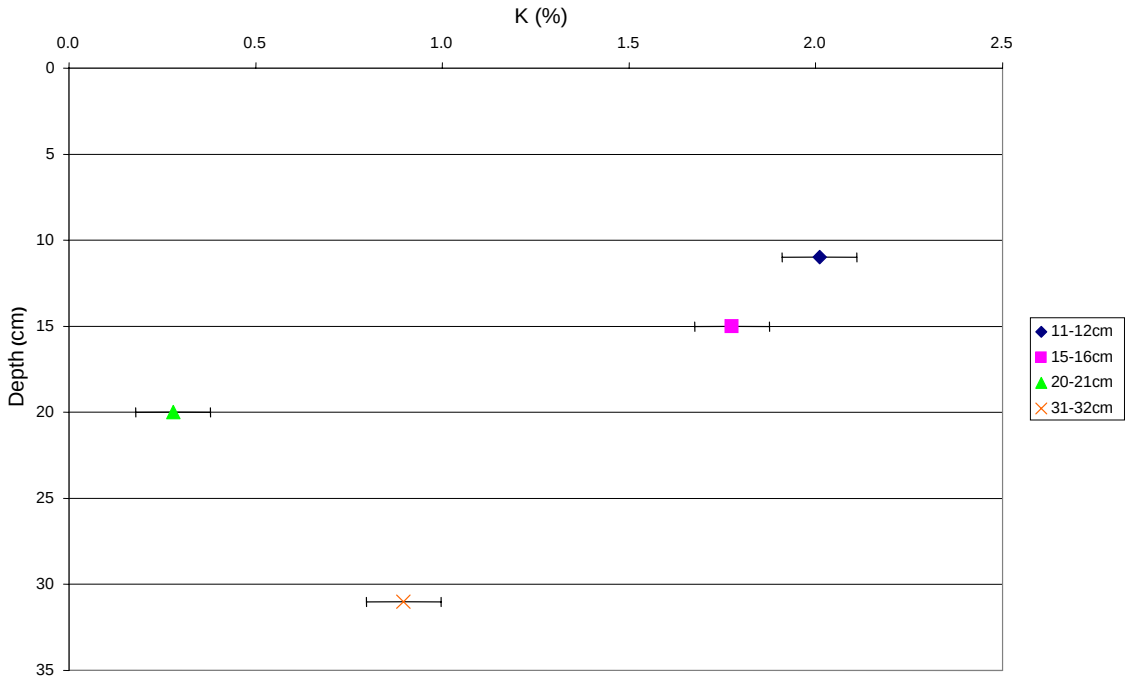

Figure 4-6. Concentration of potassium with depth in core 223BC.

Table 4-2. Specific concentrations of elements within each core

	DEPTH	^{238}U (ppm)	^{232}Th (ppm)	^{40}K (%)
CORE 249PC				
249 PCa	0–10 cm	4.5	3.1	2.5
249 PCb	0–10 cm	4.0	5.8	2.3
249 PCc	0–10 cm	4.2	5.0	2.4
249 PCclay	0–10 cm	3.9	4.3	2.7
249 PCsilt	0–10 cm	4.4	6.0	1.7
249 PCsand	0–10 cm	3.1	3.6	1.8
249 PCa	10–20 cm	4.0	4.4	2.4
249 PCb	10–20 cm	4.3	4.3	2.4
249 PCc	10–20 cm	4.6	5.2	2.4
249 PCclay	10–20 cm	6.0	4.0	2.8
249 PCsilt	10–20 cm	4.2	4.3	2.2
249 PCsand	10–20 cm	3.5	5.9	1.5
249 PCa	20–30 cm	4.1	5.3	2.2
249 PCb	20–30 cm	5.0	5.8	2.3
249 PCc	20–30 cm	4.1	6.6	2.3
249 PCclay	20–30 cm	5.3	4.4	2.7
249 PCsilt	20–30 cm	3.8	4.2	1.4
249 PCsand	20–30 cm	3.9	4.0	1.6
CORE 223BC				
223 BC	11–12 cm	3.7	4.1	2.0
223 BCclay	11–12 cm	0.1	4.2	1.2
223 BCsilt	11–12 cm	2.3	0.8	0.8
223 BCsand	11–12 cm	N/A	N/A	N/A
223 BC	15–16 cm	3.2	3.4	1.8
223 BCclay	15–16 cm	2.0	2.6	1.7
223 BCsilt	15–16 cm	2.9	5.1	1.2
223 BCsand	15–16 cm	0.2	3.9	0.3
223 BC	20–21 cm	2.4	0.6	0.3
223 BCclay	20–21 cm	2.2	2.8	1.7
223 BCsilt	20–21 cm	3.9	4.0	1.2
223 BCsand	20–21 cm	3.2	4.9	0.8
223 BC	31–32 cm	1.7	2.1	0.9
223 BCclay	31–32 cm	3.2	3.7	2.1
223 BCsilt	31–32 cm	1.9	3.2	0.3
223 BCsand	31–32 cm	0.1	0.3	0.1

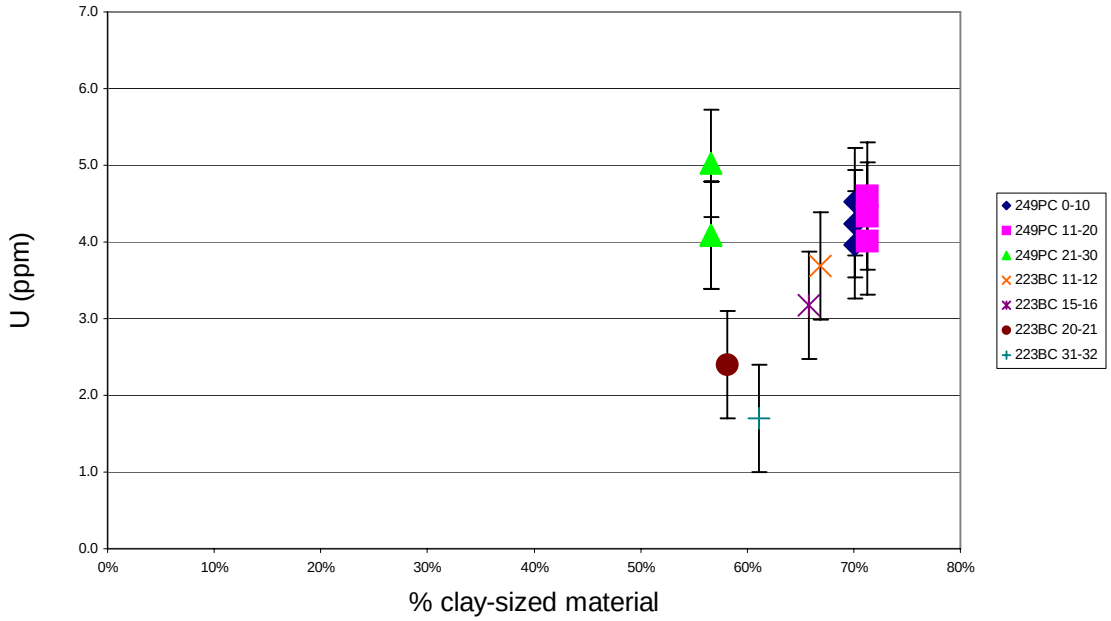

Figure 4-7. Concentration of uranium with respect to percent clay for all intervals. After ~60% clay-sized material, there is a general increase of uranium concentration with increasing clay-sized material.

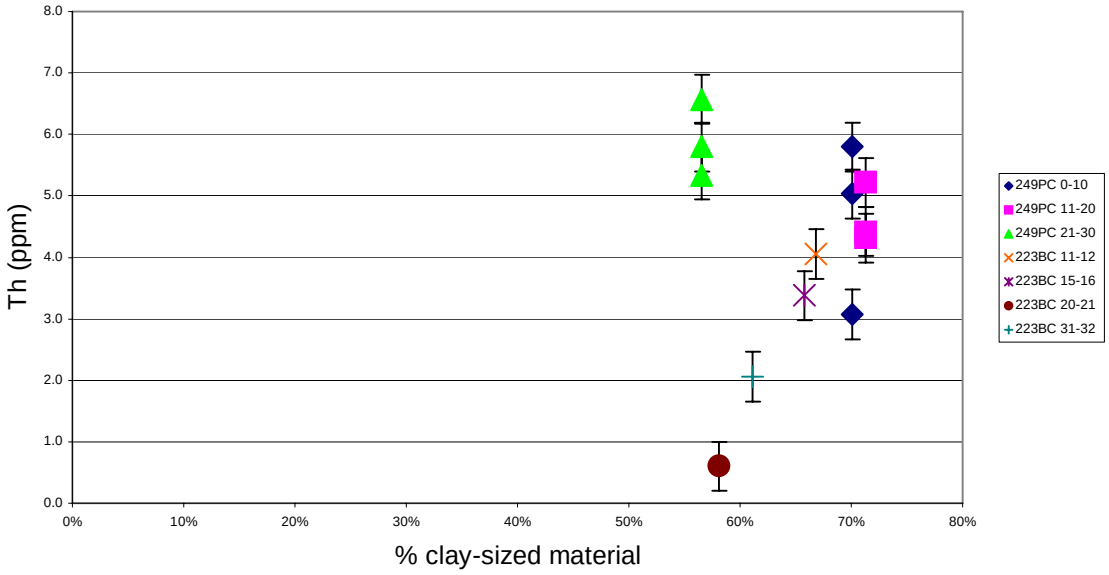

Figure 4-8. Concentration of thorium with respect to percent clay for all intervals.

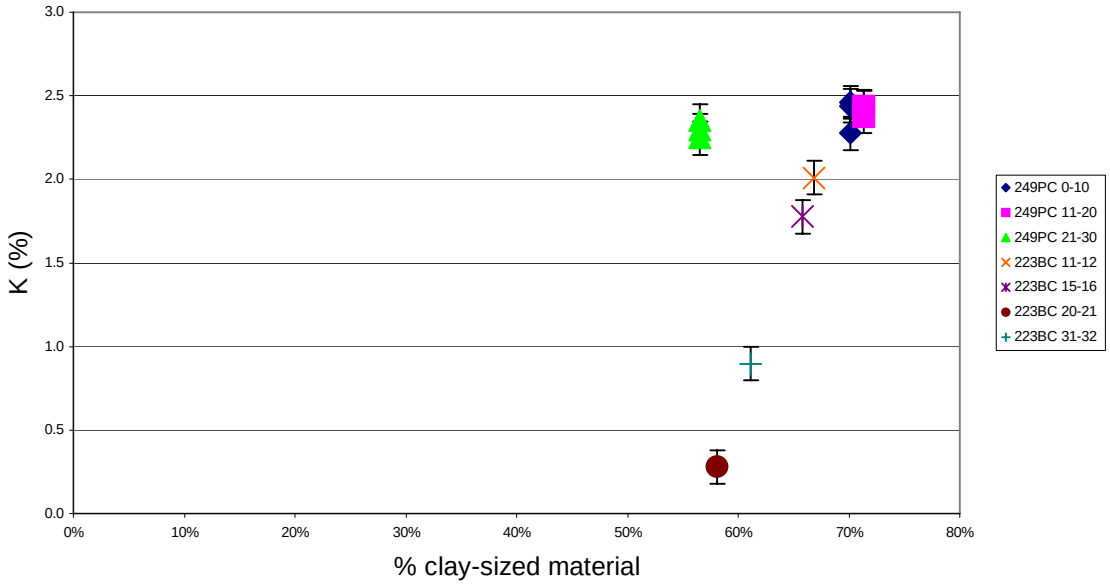

Figure 4-9. Concentration of potassium with respect to percent clay for all intervals.

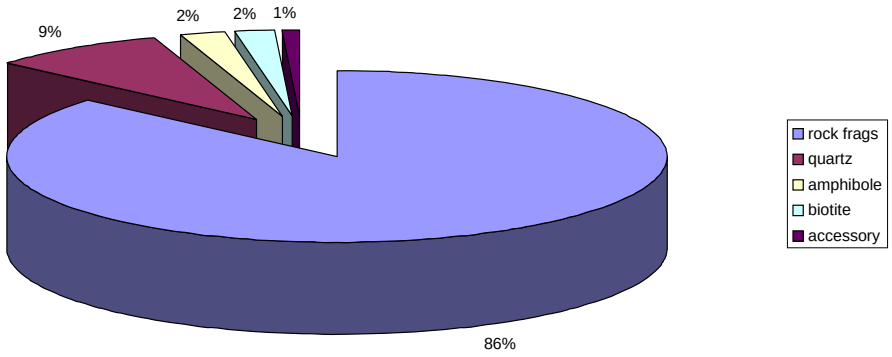

Figure 4-10. Mineralogy of sand fraction within core 249PC interval 0–10 cm.

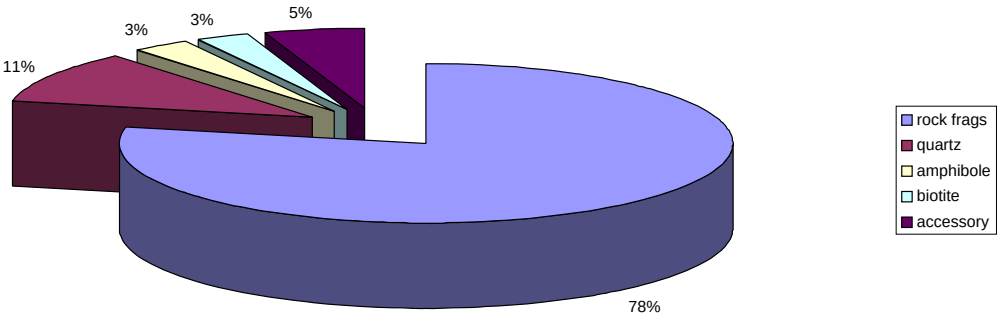

Figure 4-11. Mineralogy of sand fraction within core 249PC interval 11–20 cm.

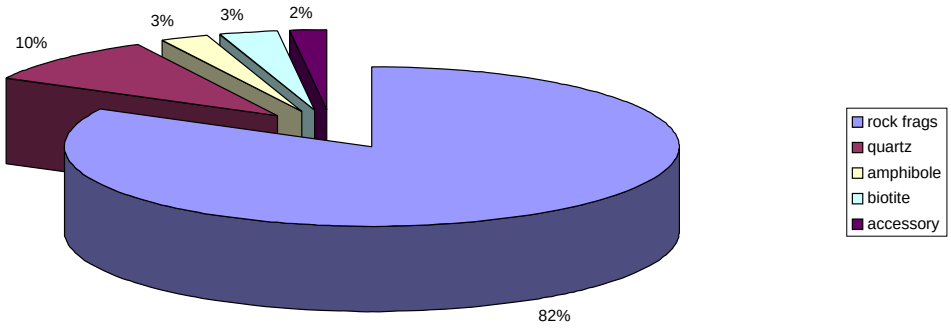

Figure 4-12. Mineralogy of sand fraction for core 249PC interval 21–30 cm.

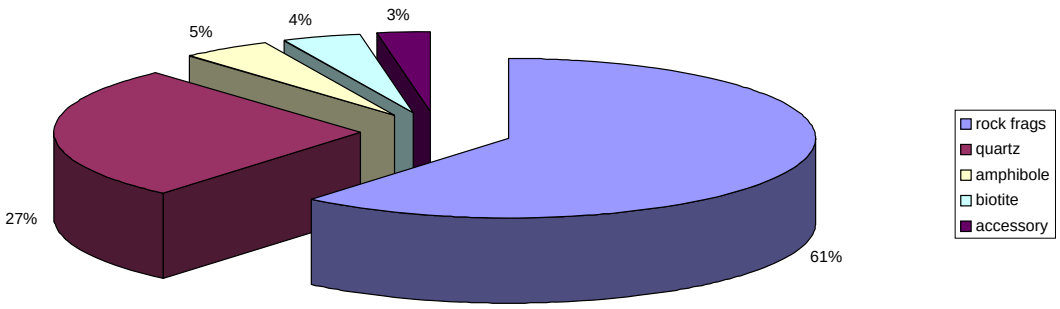

Figure 4-13. Mineralogy of sand fraction from core 223BC interval 15–16 cm.

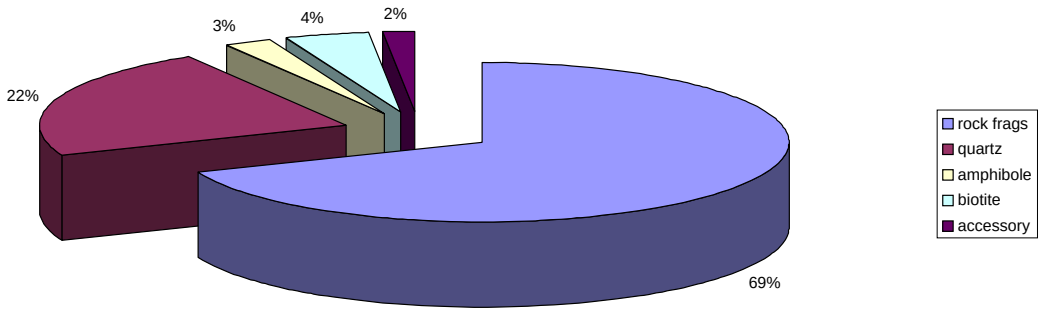

Figure 4-14. Mineralogy of sand fraction from core 223BC interval 20–21 cm.

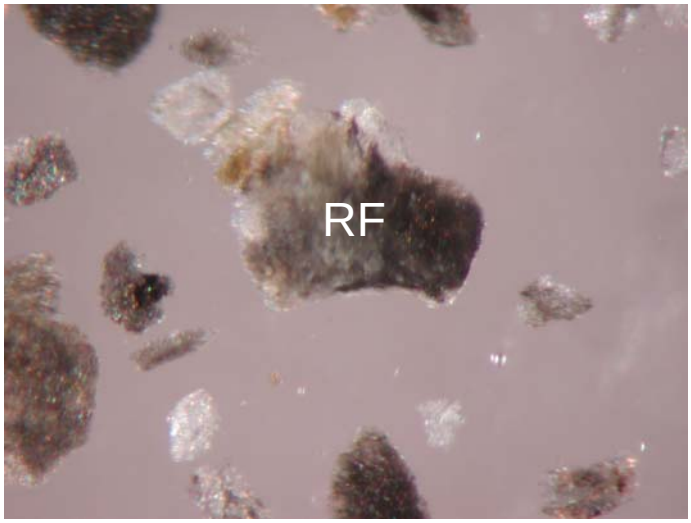

Figure 4-15. Typical image of core 249PC interval 0–10 cm showing mostly rock fragments (designated RF) with associated quartz. Field of view approximately 0.8 mm.

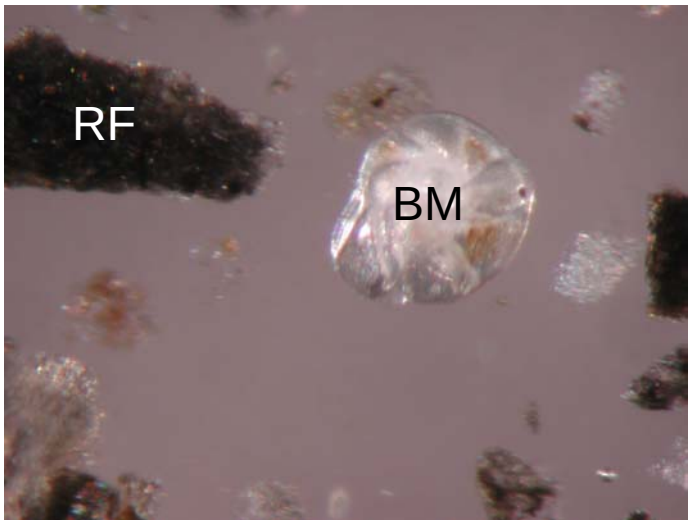

Figure 4-16. Image of biogenic material (designated BM) among rock fragments in core 249PC interval 11–20 cm. Field of view approximately 0.8 mm.

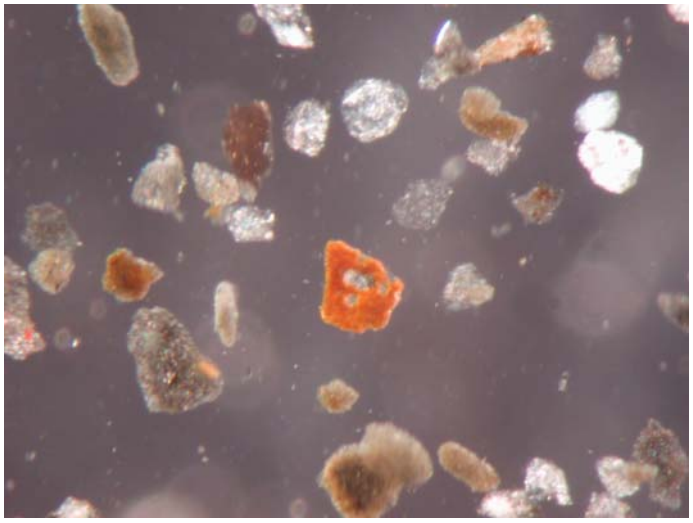

Figure 4-17. Oxidized coating on grain from core 249PC interval 11–20 cm. This interval was the only one exhibiting coated grains. Field of view approximately 1.25 mm.

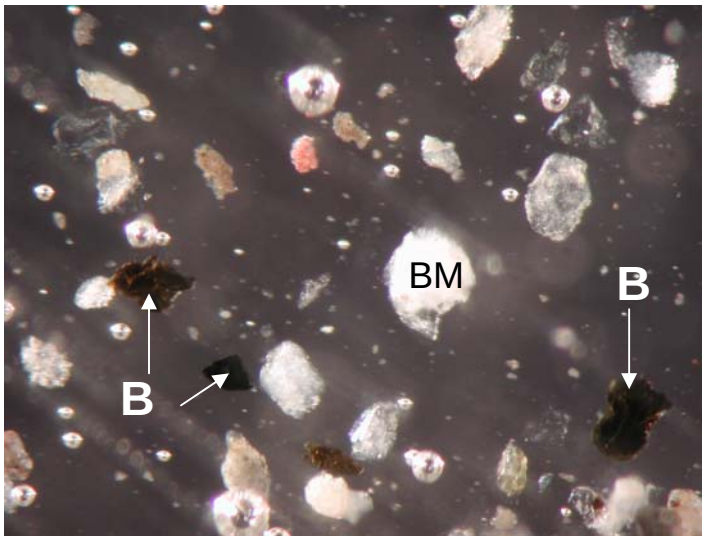

Figure 4-18. Images of biotite (designated B) and accessory minerals from core 249PC interval 21–30 cm. Field of view approximately 1.25 mm.

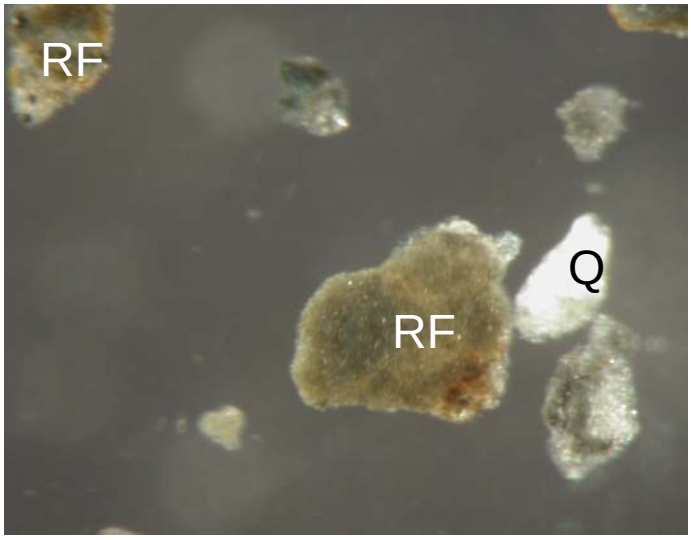

Figure 4-19. Typical picture of core 249PC interval 21–30 cm showing large rock fragments and quartz (designated Q). Field of view approximately 1.25 mm.

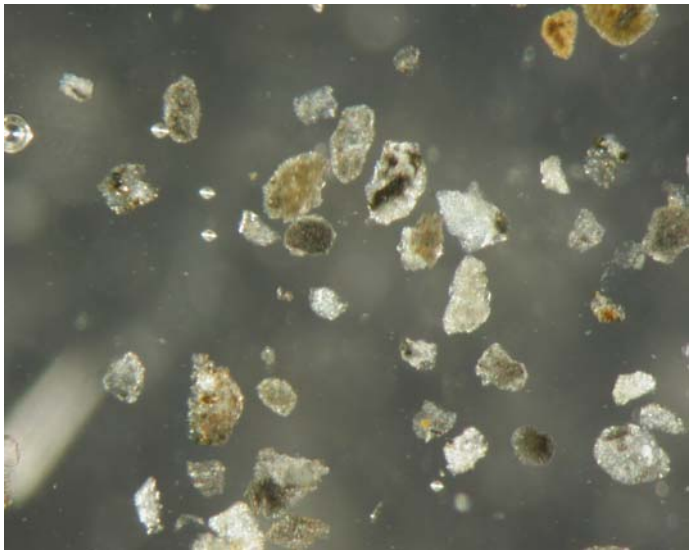

Figure 4-20. Image from core 223BC interval 15–16 cm. Rock fragments dominate but there is an increase in quartz and accessory minerals. Sand particles in this core are also more angular in shape. Field of view approximately 1.5 mm.

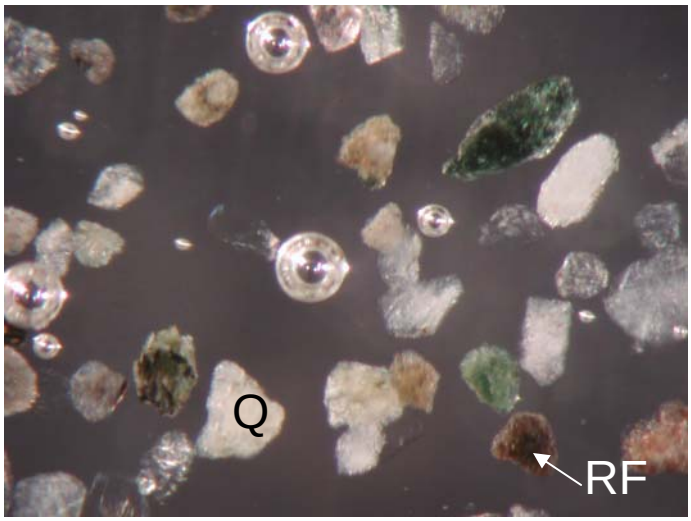

Figure 4-21. Typical image from core 223BC interval 15–16 showing elevated abundances of plagioclase and amphibole, as well as increased quartz (relative to core 249PC) among the dominant rock fragments. Field of view approximately 1.0 mm.

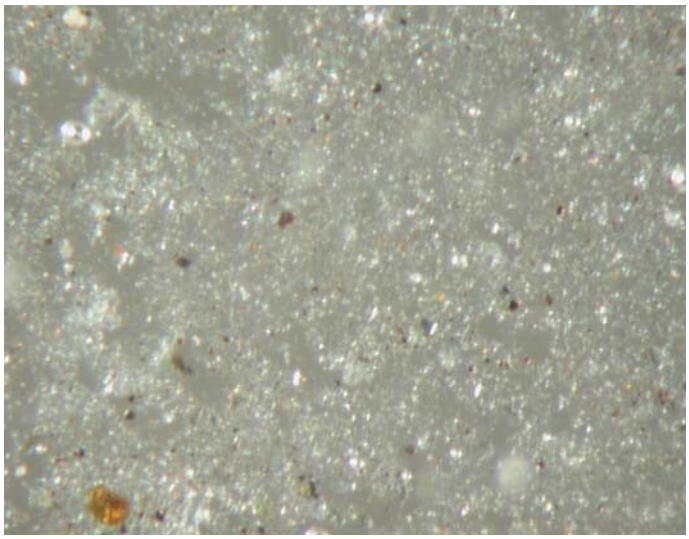

Figure 4-22. Image of core 223BC interval 15–16 cm silt fraction. Field of view approximately 1.5 mm.

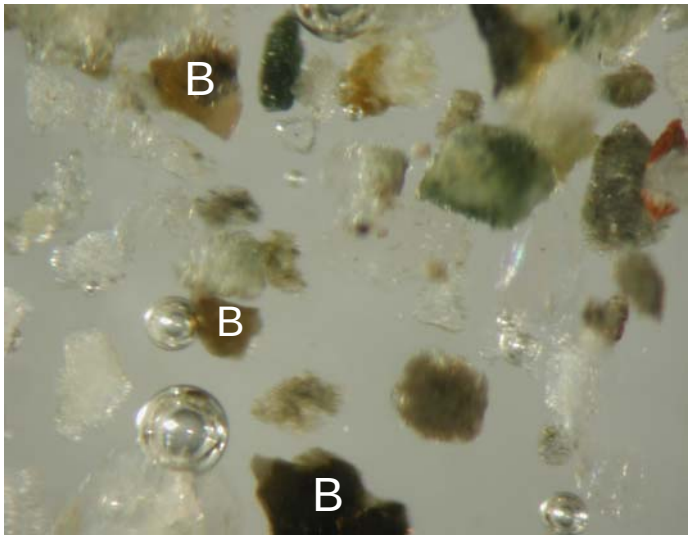

Figure 4-23. Image of biotite among rock fragments and quartz grains from core 223BC interval 20–21 cm. Field of view approximately 0.8 mm.

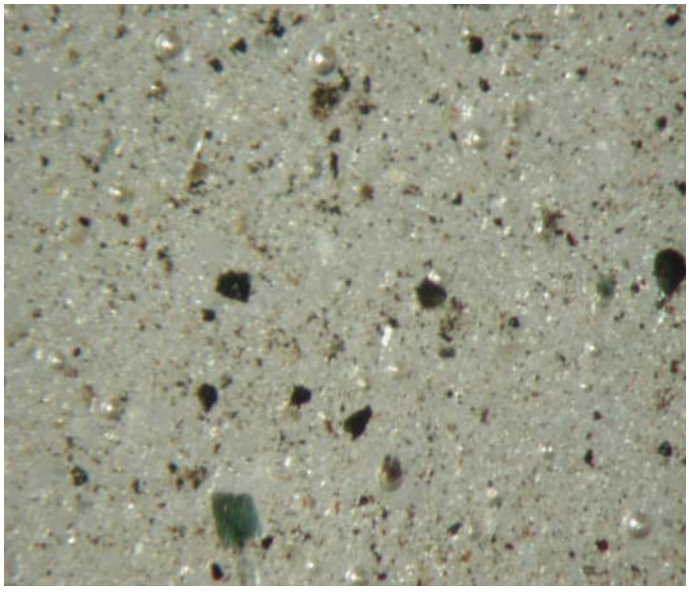

Figure 4-24. Image of core 223BC interval 20–21 cm silt fraction. The silt fragments are larger in general size as compared to the 15–16 cm interval of this core. Field of view approximately 1.5 mm.

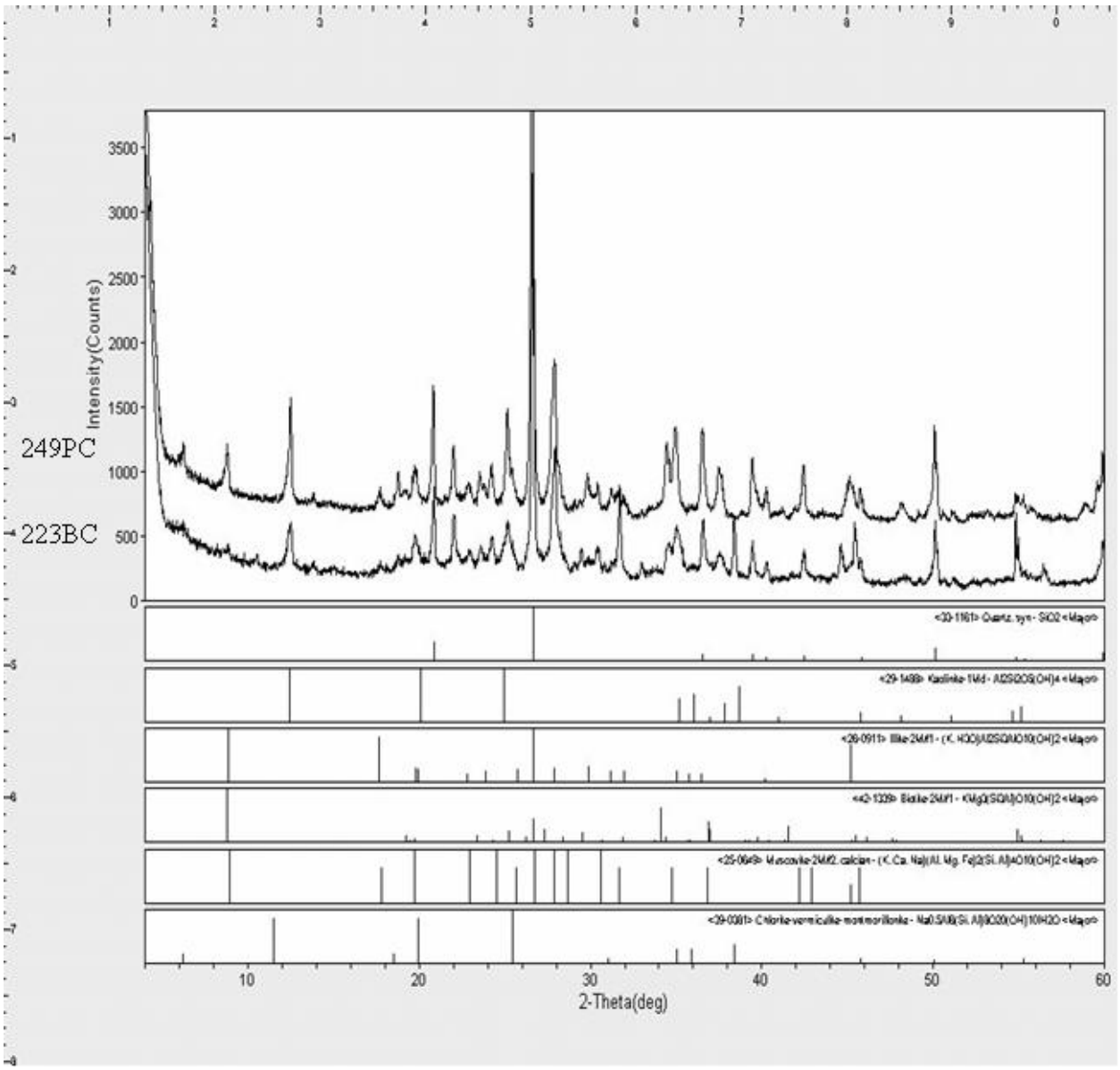

Figure 4-25. XRD data for both cores with associated mineralogy. Core 249PC is offset (raised) to better illustrate variations between cores.

Table 4-3. Percent of clay-, silt- and sand-sized fractions from the two cores. The averages for each core are included at the bottom.

	Total % clay	Total % Silt	Total % Sand
249PC			
0–10cm	70	22	8
11–20cm	71	25	4
21–30cm	57	31	12
223BC			
11–12cm	67	31	2
15–16cm	66	30	4
20–21cm	58	36	6
31–32cm	61	39	0.3
Averages			
	Avg. clay %	Avg. silt %	Avg. sand %
249PC	66	26	8
223BC	63	34	3

CHAPTER 5
DISCUSSION

Grain Size

Core 249PC has a similar percentage of fine-sized sediment in the 0–10 and 11–20 cm intervals, with a decrease in sand due to a slight (1% and 3%) increase in clay and silt. The 21–30 cm interval exhibits a significant drop in clay and increase in sand from the two intervals above it. This influx of sand can be attributed to the 1964 earthquake, which corresponds to that interval given the sediment accumulation rate (~1 cm y^{-1}, Jaeger et al. 1998). The earthquake epicenter was located in nearby Prince William Sound and accounted for extensive redistribution of sediments by tsunamis (Jaeger et al. 1998).

Sand percentage at core 223BC increases steadily downcore (2%, 4%, and 6%) until the 31–32 cm interval where it drops to 0.3 %. Due to the extremely high sedimentation rate in the northern Icy Bay location (>0.3 cm d^{-1}, Jaeger 2002) and lack of steady-state deposition, inconsistencies with accumulation and grain size at depth are expected. Decreased sand could be attributed to increased precipitation, which may substantially increase meltwater discharge and associated velocity, and allow for deposition of the sand-sized fraction further from the glacial termini.

The two sites reveal variations in transport environments, which may affect grain size distribution. The presence of a moraine and Bear Lake between Bear Glacier and the Resurrection Bay core 249PC site may act as a trap for grains silt-sized and larger, whereas Guyot Glacier is a tidewater glacier, which deposits sediment directly into Icy Bay (Figs 2-1, 2-2). This may also explain the lower relative clay percentages in core 223BC compared to core 249PC. Guyot Glacier is connected to the water body and contributes sediment directly into Icy Bay, allowing for extended suspension and distribution of the finer particles.

Composition

Mineralogy of the two cores is surprisingly similar. Both cores are from a temperate glacial environment in the GOA, which produces predominantly glacimarine rock flour, therefore, a general similarity in particle size and common rock-forming mineralogy (relative to other parts of the world) is expected. The almost identical results from both petrographic and XRD analyses are not expected based on differing source lithology and geological environments (Figs. 1-2, 1-3). The XRD patterns, when viewed together, are distinguished only by more well-defined peaks from the Icy Bay sample, and one or two additional minerals (likely feldspars, McClellan, verbal communication) at the same site (Figure 4-25). Differences in peak intensities are partly due to variations in clay mineralogy as well as increased overall clay percentage in the 249PC sample. Higher proportions of clay-sized particles produce a less intense, muted appearance in graphs (Moore and Reynolds 1997). The mineralogic analyses (4-10 through 4-14) show nearly identical sediment compositions, even with regard to accessory minerals. The variation is principally in relative percentages, the exception being the increase in biogenic material under accessory minerals in core 249PC interval 11–20 cm. These findings indicating that the source rocks presented in the two core sites may not be as different as initially thought. No source has currently been determined for the Yakataga Formation. It is possible that the Chugach terrane, which is the source material for core 249PC sediments, is also the source for the Yakataga Formation sediments of core 223BC.

The point count data for core 249PC shows an overall decrease in rock fragments with depth, and a slight elevation in amphibole, biotite, and accessory minerals for intervals 11–20 cm and 21–30 cm. The coarse-size fraction of both cores contains predominantly rock fragments, with the next most common occurrence being quartz (though core 223BC consists of nearly twice the quartz of core 249PC). Both cores also contain biotite, amphibole, and accessory

minerals in amounts of less than 5 percent. The weathering of differing source rock types surrounding each basin should hypothetically produce differing clay-mineral percentages (Hein et al. 2003). Though relative clay-mineral percentages vary between the cores, it is only a slight variation which can be attributed to differences in sedimentation processes between core sites, or seasonal sediment discharge fluctuations. Elevated illite content at the Resurrection Bay area relative to the Icy Bay area seen in the XRD analysis was also recorded by Molnia and Hein (1982). A single depositional or aperiodic event might alter source of sediment, and is a possible reason for elevated illite (e.g., flooding at an illite-rich drainage basin or rapid draining of a lake).

Elemental Concentrations

Elemental concentrations are predominantly due to mineralogy, diagentic changes of clay mineralogy, and adsorption processes (Ayres and Theilen 2001). Elevated clay mineral contents (illite, chlorite) and overall clay-sized material percentages in core 249PC (Figure 4-25, Table 4-3) correspond to higher isotopic concentrations. Radioactivity is often associated with clay- or fine-sized particles (van Wijngaarden et al. 2002, Anderson 2004, Naidu, Han, Mowatt, and Wajda 1995). Relatively high concentrations of K have been recorded in marine sedimentary rocks of the Valdez Group near Bear Glacier (Goldfarb and Borden 1982). The Aialik pluton outcrops discontinuously around the mouth of Resurrection Bay, it is locally biotite-rich and may contribute to increased potassium levels (Kusky, Bradley, Donley, Rowley, Haeussler 2003).

In an attempt to better represent elemental concentrations, samples from this study were normalized to percent clay. (Table 3-2) Due to the high amount of clay initially in most of the intervals, relative concentrations of normalized data are similar to initial bulk concentration data, with an increase in specific concentrations. Core 249PC interval 21–30 cm has a high elemental concentration (in each of the three elements) with respect to the relatively low sand percentage

(Figs 4-7 through 4-9). This may be due to the catastrophic nature of the 1964 earthquake event that deposited the sediment. Material of a wide range of sizes was moved at an extremely rapid rate, which would allow for minimal disaggregating of clay particles before deposition and burial.

^{238}U

Though the averaged concentrations for uranium in core 249PC show an increase in activity with depth, it is not definitive. (Figure 4-1, Table 4-2). Based on the concentration data and associated errors (Figure 4-1), it is impossible to conclude there exists an increased uranium concentration with depth. There is, however, a general consistency of uranium elemental concentration in all intervals from core 249PC, even at the 21–30 cm interval, which contains considerably less clay. By analyzing a homogenized 10 cm sample, as was done for core 249PC, fluctuations in sedimentation could be minimized, producing more consistent results.

The uranium concentrations in core 223BC decrease with depth in an almost linear manner. The decrease in concentration corresponds to a decrease in clay and, therefore, supports the correlation of activity of this element with grain-size. At the 20–21 cm interval uranium is elevated relative to thorium (Tables 4-1, 4-2). This interval is the most similar to the hypothesis put forth regarding an increase in uranium with associated decrease in potassium and thorium, and is the only interval where this behavior is seen. The hypothesis stated this might be due to heavy minerals concentrated in the sand fraction. Based on the mineralogy observed in this study that conclusion is unlikely.

^{232}Th

Core 249PC shows an increase in the average concentration of thorium with depth. When errors are taken into account (Figure 4-2) the increase becomes unclear. This results in thorium exhibiting a general consistency in elemental concentration among all intervals, much like the

uranium concentration in this core. There is an increase in silt content (Table 4-3) with depth that may support the association of thorium with the silt-sized fraction. Due to lack of consistency, it is more accurate to associate thorium with the more general fine-sized fraction (<63 μm) than to specify either the clay- or silt-sized fraction. Thorium elemental abundance in core 223BC shows the same general decrease with depth as seen with uranium, except at the 20–21 cm interval where concentration significantly lower than the other intervals. Thorium abundance in both cores is higher than uranium abundance, and can be related to initial mineralogy, since thorium is more abundant in the earth (10ppm) than uranium (2ppm) (Ruffell and Worden 1999). This interval exhibits the highest amount of sand (6 %) within the core, supporting the association of the fine-sized fraction with thorium elemental concentration. The elevated thorium concentration relative to uranium at both the Resurrection Bay and Icy Bay core sites is also seen in published geochemical data. (Figs. 1-4 through 1-6)

^{40}K

The percentage of potassium in core 249PC fluctuates very little (<1 %) and, therefore, does not specifically show a decrease with depth. Potassium concentration only varies by 0.1% in each of the three intervals in the 249PC core. The concentration is highest in the clay fraction and lowest in the sand fraction at every interval. The consistency seen in potassium elemental abundance among samples for core 249PC is similar to uranium and thorium. The sediment associated with core 249PC shows slightly elevated overall concentrations of all radioisotopes examined when compared to core 223BC, but is particularly noticeable with potassium.

Core 223BC potassium concentrations range from 0.3 % (20–21 cm interval) to 2.0 % (11–12 cm interval). Core 223BC shows an overall decrease in potassium with depth, similar to the uranium and thorium concentration with depth seen in this core. The exception is a very low

concentration at the 20–21 cm interval which corresponds to the lowest amount of clay (58 %) and highest amount of sand (6 %) in the core.

There is an obvious association of potassium with the clay fraction for both cores. Glacial meltwater is known to be relatively high in potassium (Anderson 2004). Sediment discharged into the GOA is predominantly clay-sized and thus is the principal potassium source, since potassium is locked in the clay mineral lattice and relatively immobile. Physical grinding of biotite grains during abrasion in this type of glacial environment also exposes the inner layer (potassium) cations (Anderson 2004). The release of potassium relative to plagioclase is promoted in colder climates due to this type of biotite weathering (White et al. 1999; Blum and Erel 1997) and thus contributes to overall potassium. The potassium radioisotope is spread through many rock-forming minerals (e.g., feldspar) as well as heavy minerals (Asadov, Krofcheck, and Gregory 2001), so a uniform signal even after separation into size fractions is not uncommon.

In general, core 249PC exhibits a different (elevated) elemental abundance from that of core 223BC, particularly when normalized to mass percent clay (Table 3-2). The distinction can be associated with an elevated percentage of clay-sized grains at core 249PC (Table 4-3), since there is an association of concentration with the fine-sized fraction. Note that the low sand content in the 11–20 cm interval does not result in a low uranium concentration or elevated thorium and potassium. A higher accessory mineral content was recorded for this interval, but was largely due to increased diatom tests and biogenic material. The initial hypothesis suggested that ^{238}U (uranium) in the cores was associated with zircons or other heavy minerals which are resistant to weathering and, therefore, concentrated predominantly in the coarse (>63 μm) fraction, and that ^{232}Th (thorium) and ^{40}K (potassium) are associated with clays (illite, chlorite)

and mica. Uranium abundances are similar to thorium and potassium abundances at almost every interval. The intensity of the glacial abrasion can promote the release of dissolved uranium from rocks into the waters where it would be incorporated into the fine-sized fractions (Taboada, Cortizas, Garcia, and Garcia-Rodeja 2006; Hodson 2002).

The decrease in percent clay at the core 223BC 20–21 cm interval is a likely explanation for lower ^{232}Th and ^{40}K activities. Gamma-ray activity should be a function of grain size (Asadov et al. 2001), and appears to be recorded here. With regard to potassium in particular, there seems to be an association with the fine-sized fraction, (the dominant sediment mode in the GOA), and the clay-sized fraction specifically. Changes in clay mineralogy (decrease in potassium-rich illite clay relative to smectite clays) are thus likely responsible for decreasing natural gamma activities not associated with decrease in clay-sized sediments.

Clay Mineralogy

Clay mineral assemblages play an intricate role in controlling radioactivity and are particularly informative of source rock composition (Naidu et al. 1995). This is primarily due to the fine-sized fraction comprising the majority of sediment discharged in the GOA and the association of potassium with this fraction (Jaeger et al. 1998; Molnia and Hein 1982; Anderson 2004). Clays in the GOA are characterized by high amounts of illite and chlorite with traces of expandable clay minerals and little to no kaolinite (Naidu et al. 1995; Molnia and Hein 1982). Based on XRD in this study there is a presence of kaolinite that is considered to be high relative to previous studies. This is attributed to kaolinite having a tendency to flocculate and concentrate in shallow marine successions close to shore (Ruffell and Worden 1999). Kaolinite and expandable clays such as montmorillanite contain significantly less potassium (and thorium) relative to illite clays (Ayers and Theilen 2001; Ruffell and Worden 1999). Thus, if a decrease in the relative abundance of an element (e.g., potassium) does not coincide with a significant

decrease in the fine-sized fraction, it may simply be related to the clay minerals present, as well as the mineralogy of non-clay minerals in the clay-sized fraction.

Th/K Ratios

It is suggested that the mobility of potassium and uranium and the relative concentration of thorium during weathering should result in clays with elevated Th/K and Th/U ratios (Schnyder et al. 2005). The Th/K ratio is used to recognize clay mineral, feldspar, and mica associations (Ruffell and Worden 1999). Clay mineral analyses and Th/K ratios help to distinguish long-term transgressive events as well as short-term flooding (Ruffell and Worden 1999). When these ratios are plotted, core 249PC exhibits a mix of chlorite and illite, with most points falling close to each other due to the very consistent potassium concentration. (Figs 5-1 through 5-3) Core 223BC shows a very consistent ratio of 2:1 for thorium and potassium. Core 223BC interval 20-21 cm records the lowest concentration of both thorium and potassium. When the Th/K ratio is plotted against percent clay, there is little distinction between the two cores. (Figure 5-4) The similarity of clay mineral percentages, as well as depositional processes would produce similar Th/K ratios once normalized to clay.

Possible Alteration/Biasing of Signal

It is important for this study to understand the potential extent of chemical weathering in the glacial environment, particularly for this type of study, which assumes initial source material is represented accurately in the sedimentary record. The geochemistry of a sedimentary deposit is often influenced by many variables other than parent rock composition (Fralick 2003). Weathering can be the dominant process affecting the geochemistry of sedimentary rocks, and physical weathering is the dominant process in glacial environments. Mobility of elements is particularly hard to constrain in these types of cold weather environments. Uplift and erosion are actively occurring in the GOA, and they are a driving function for geochemical cycling.

Additionally, runoff and temperature are two of the most important parameters controlling chemical weathering rates (Dessert, Dupre, Gaillardet, Francois, and Claude 2003; Derry and France-Lanord 1996). The nature of the temperate glaciers within the study area makes chemical alteration a possibility relative to colder climates due to the presence of water at the glacier base. This allows the glacier to erode its bed and thus provides conditions necessary for accelerated weathering (Anderson, Drever, Frost, and Holden 1999).

The potential of a difference in uranium concentration between parent-rock and sediment deposited is greater than that of thorium or potassium in this type of environment (Ruffell and Worden 1999). Conditions on the southern Alaska margin are considered oxidizing and there is very little organic matter present. Under sufficiently oxidizing conditions uranium is commonly soluble in water (as U^{+6}), while thorium has low solubility (Faure 1986). The mineralogy of the sand fraction did not reveal heavy minerals typically associated with uranium and therefore must be broken down prior to deposition and incorporated into all size fractions. This even distribution could occur by dissolved uranium in the water column being transported in proglacial rivers and streams. Thorium and potassium are both considered to be locked in the mineral lattice, and relatively immobile. The exception is thorium, which may be somewhat mobile in the water column.

The GOA is considered an oxidizing environment, it is likely that reducing conditions would exist only after deposition. Post-depositional alterations are very unlikely considering the rapid accumulation of sediment at each site, and relatively short time-period represented in each core. Previous studies show that glacial meltwater is likely the dominant factor governing elemental fluxes (White and Blum 1995; Anderson 2004). There are englacial and supraglacial flow paths transmitting water quickly to outlet streams, allowing little opportunity to interact

with rocks and sediments (Anderson et al. 1999; Collins 1979). Mountain ranges in very close proximity to the sea such as in southern Alaska minimize terrestrial storage, and sediments within the Gulf have previously been characterized as having undergone mild chemical weathering (Jaeger et al. 2001; Anderson 2004). Alteration is possible, but considered unlikely and very mild given the extremely high discharge rates.

Correlation with Aeroradiometric Data

Aerial gamma-ray surveys measure the flux of gamma-rays emitted by the radioactive decay of the elements ^{40}K (potassium), ^{238}U (uranium), and ^{232}Th (thorium). These elemental abundances can be used as proxies for studies, because different rocks and soils generally contain different amounts of these elements. Thus the aeroradiometric measurements obtained can be useful for locating intrusive rocks and mapping rock units with a distinctive radioelement signature (Duval, Cook, and Adams 1971). The National Uranium Resource Evaluation (NURE) program was conducted by the U.S. Government to assess radioelement data (Duval 2001). The program included airborne gamma-ray spectrometry and magnetic data collection along with extensive geochemical sample collection and processing. Aeroradiometric surveys of 98 1° by 3° quadrangles were flown in Alaska between 1975 and 1980. The data, collected in 15 surveys flown approximately 400 feet high and spaced approximately 6 miles apart, were done by Texas Instruments (T.I.), Lockwood, Kessler and Bartlett (LKB), and AeroServices (Aero) under contract with the U.S. Government. The surveys typically penetrate the upper 2 feet (Duval et al. 1971).

There is little correlation with aeroradiometric data in this study. (Figure 1-7) Elevated uranium measured in sediments at the Resurrection Bay site (relative to Icy Bay) are not depicted on the aeroradiometric map. There is a small area on the survey map near Resurrection Bay which shows the presence of uranium, though it would not seem to be enough to influence the

elevated concentration recorded in the sediment here, particularly when compared with those of the Icy Bay core. The aeroradiometric survey map shows an absence of thorium in the Icy Bay environment with a highly elevated uranium concentration, also not recorded in the measured data.

One possible explanation for the elevated uranium concentration near Icy Bay on the aeroradiometric map is the preferential sorting of heavy minerals by aeolian transport processes. Aeolian transport has been shown to be effective at zircon enrichment and produce very high Zr and Hf contents in loess deposits when compared to continental crust (Taylor 1983; McLennan et al. 2003). These zircon enrichments on the surface near the Icy Bay environment would cause elevated uranium unrelated to parent rock material or the coarse fraction. There might also be biases in the aeroradiometric map due to extrapolation of data. The 6-mile spacing between flight-lines would require assumptions to be made about the areas not directly measured. The analysis then is that there is no overall correlation of aeroradiometric maps with measured concentrations, and they should not be used for comparison with core material in the southern Alaska environment.

Correlation with Geochemical Data

Geochemical data from river and stream samples (Figs. 1-4 through 1-6) reveal very similar elemental abundances to those determined at the core sites. The thorium data suggest a concentration at both core locations with a range from <3.7 to 8.7 ppm. (Table 4-1) Thorium concentrations were slightly lower at core 223BC relative to core 249PC, but still fall within published ranges. Potassium concentrations of both published data and that of this study show elevated concentrations in the core 249PC environment relative to those at core 223BC. Uranium is also slightly elevated in both this study and published data at the 249PC site. Core 223BC published data suggests a concentration ranging from approximately 1.4 to 3.8 ppm,

which is very close to what this study observed. The environment near core 249PC shows a range of 1.9 to 7.3 ppm in published data, which is also almost identical to what was observed in this study. Though the ranges for core 223BC are large relative to 249PC ranges, they are well within the concentrations of published geochemical data.

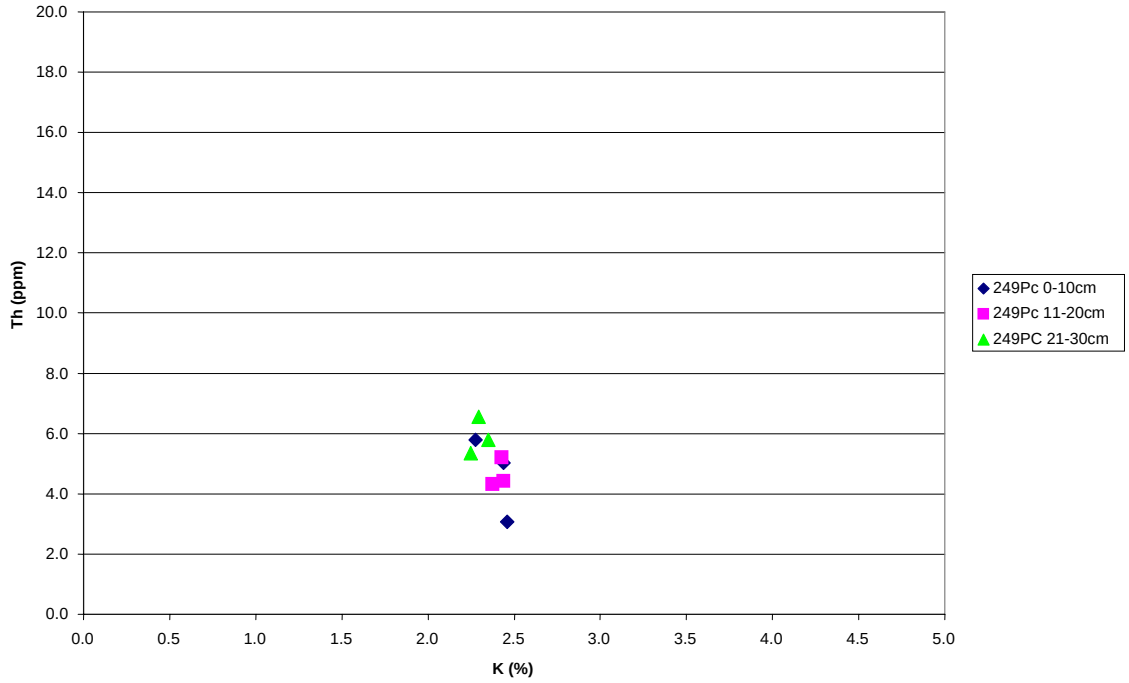

Figure 5-1. Th/K ratio from core 249PC.

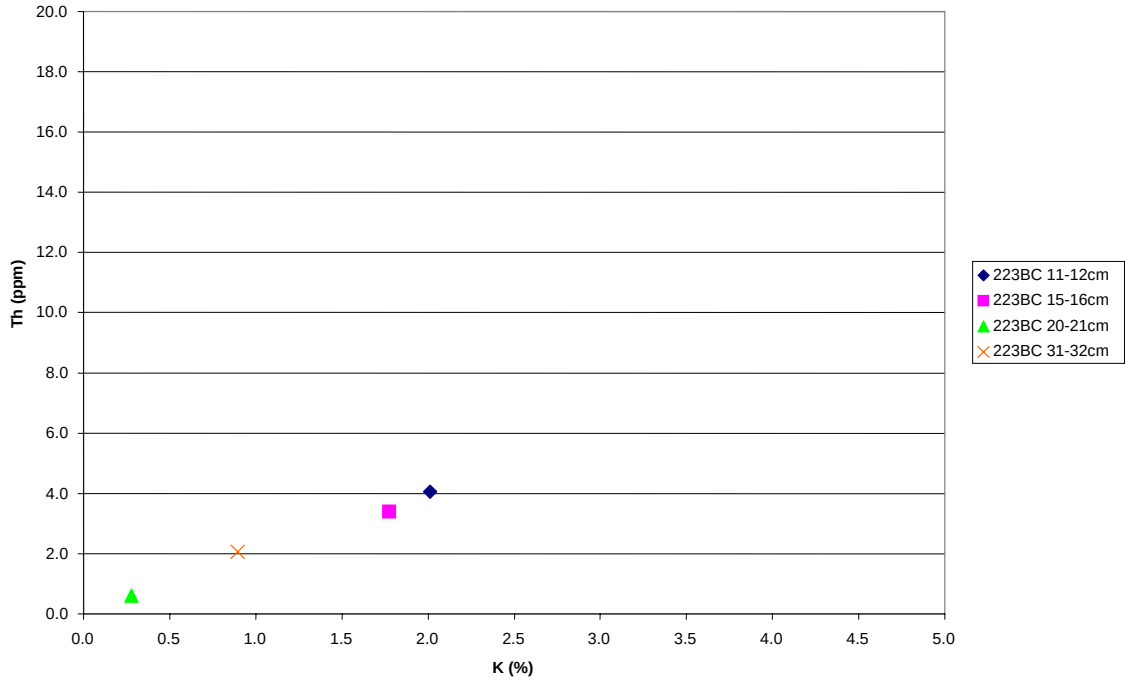

Figure 5-2. Th/K ratio for core 223BC.

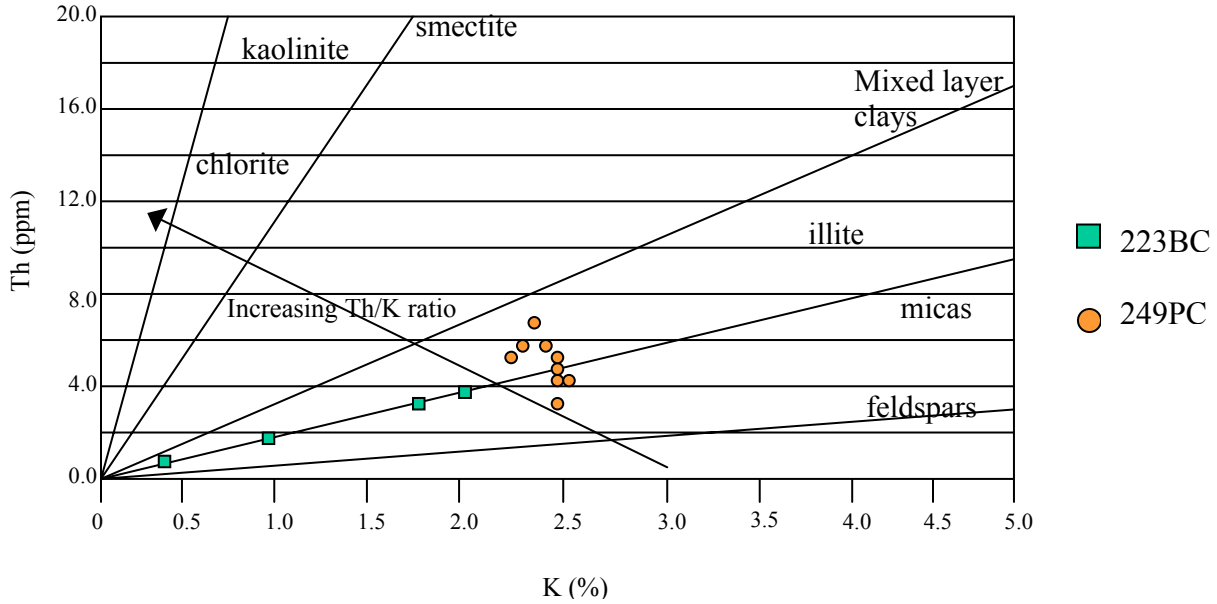

Figure 5-3. Overlay of Th/K ratio for both cores

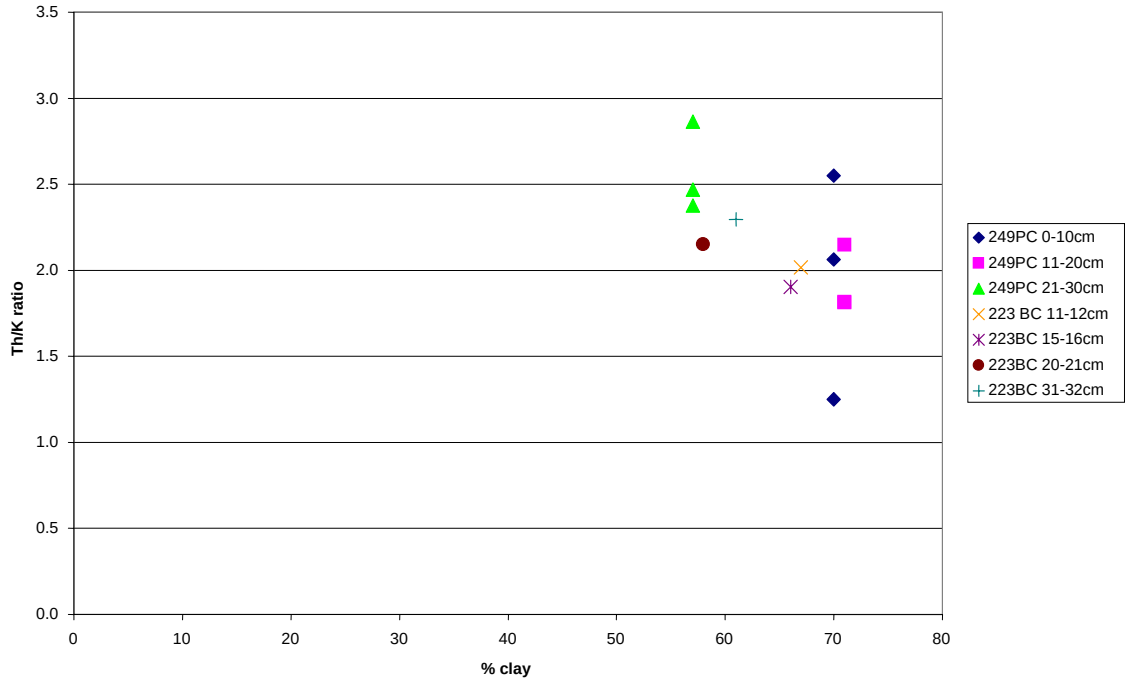

Figure 5-4. Th/K ratio with percent clay for cores 223BC and 249PC showing little variation between them.

CHAPTER 6
CONCLUSION

The hypothesis stated previously was that ^{238}U was associated with zircons or other heavy minerals carried predominantly in the coarse (>63μm) fraction, and that ^{232}Th and ^{40}K were associated with clays (illite, chlorite) and mica in the fine-sized fraction. This was expected to produce an elevated ^{238}U concentration in core 223BC, and an elevated ^{232}Th and ^{40}K concentration at core 249PC, since 249PC contains more fine-grained material. Though 249PC did show elevated ^{232}Th and ^{40}K concentrations due to a higher clay percentage, the ^{238}U was also increased. This is indicative of the ^{238}U radioisotope also being carried predominantly in the fine-sized fraction.

This study shows no correlation between concentration and the sand-sized fraction. The sand fraction has been shown to display a wide range of radioactivity and often produces results similar to those in this study (Blum and Erel 1997; Ayers and Theilen 2001). The variability of ^{238}U and ^{232}Th with each interval makes it difficult to discern precisely where it is being carried, though it is can be generally associated with the fine-sized fraction. There is particularly good association of the ^{40}K radioisotope with the clay-sized fraction, it is highest there for each interval of both cores. Natural gamma activity in this study is thus controlled primarily by grain size and not mineralogy, though clay mineral assemblages do play a role in determining relative amounts of potassium. Previous studies have determined that the radioactivity from potassium often dominates the natural activity of the sediment and can be used as a provenance tool (Ayers and Theilen 2001).

The second part of the hypothesis suggested that if grain size did play a role in controlling radioisotopic activities, then it could be possible to determine provenance based on the radioisotope analysis of each core. Though grain size does show a strong correlation with

potassium, the similar overall clay percentage and mineralogy of the two cores make a distinct provenance determination difficult. Overall concentrations of core 249PC are higher than those of core 223BC are therefore distinguishable, but not convincingly. It is very possible that the Chugach terrane associated with the Chugach and St. Elias Mountains is influencing the source material at both locations, thus disrupting the unique geological terrane characteristics. This would imply that the Valdez group and the Yakataga formation are composed of material from the Chugach terrane. Specific determination source material for the Yakataga formation is beyond the scope of this thesis, however, the similarity in XRD and petrographic analyses supports a more similar source material than originally estimated. The slightly elevated radioactivity at core 249PC is then attributed to a combination of elevated fine-sized sediment and slightly elevated initial potassium content of the rock assemblages near Bear Glacier and Resurrection Bay.

A secondary goal of the study was to test the validity of aeroradiometric data from the southern Alaska region. The noticeably high uranium in core 223BC relative to 249PC illustrated in Figure 1-7 was not seen. This is likely due to the misrepresentation of parent rock material by aeroradiometric data. The high uranium levels recorded are attributed to concentrated near-surface coarse material deposition both by receding glacial activity and aeolian processes. This would concentrate heavy minerals that weren't incorporated into the finer fraction (such as zircons and monazite) in the coarse fraction while the fine-sized fraction was transported to the Gulf. Certain storm-induced flooding resulting in high sediment discharge will still carry some heavy minerals to the Gulf (possibly recorded in core 223BC interval 20–21 cm), however would not be significant enough to prevent a bias in aeroradiometric measurements at certain depositional environments. Inferring sediment provenance from the

final product is anything but straightforward since it evolves as it is transported from the source, this affects the near-surface sediments measured by the aeroradiometric surveys in particular (Weltje and Eynatten 2004).

This study shows that, in general, there is a correlation of radioisotope activity with grain size. The inconsistencies observed reveal there are other factors, such as mineralogy and surface adsorption (particularly for ^{232}Th), contributing to overall activity. Activity of the ^{40}K isotope is the least affected by factors other than grain size, and correlates well with the amount of clay-sized material. The similarity of source mineralogy makes distinction between locations difficult. Results do show a slight distinction the two cores, and thus it may be possible to use this technique for provenance determination between two more unique environments. Th/K ratios are consistently near 2:1 at core 223BC, whereas the ratio at core 249PC is variable. Also, the minimum ^{40}K values of core 249PC are higher than the maximum ones at 223BC. Natural gamma activity in this study is then primarily controlled by amount of clay minerals and the potassium content of the clay mineral assemblages, which has been recorded in other studies (Ayres and Theilen 2001; Carter and Gammon 2004). Naturally it would be ideal to apply a suite of current techniques to obtain the highest accuracy and precision for provenance determination. These techniques can be very time consuming and expensive. Geochemical data from stream and river samples (Weaver 1983) for the GOA margin correlates well with radioisotopic concentrations measured in this study, proving that it is a non-destructive and efficient way of accurately determining radioisotope concentration. Given two more unique environments, this technique could be a very valuable provenance tool.

LIST OF REFERENCES

Andersen, T., 2004. Detrital zircons as tracers of sedimentary provenance: Limiting conditions from statistics and numerical simulation. Chem. Geol. Science Direct online, Dec. 2004.

Anderson, S.P., Drever, J.I., Frost, C.D., Holden, P., 1999. Chemical weathering in the foreland of a retreating glacier. Geochim. Cosmocim. Acta 64, 1173-1189.

Anderson, S.P., Longacre, S.A., Kraal, E.R., 2003. Patterns of water chemistry and discharge in the glacier-fed Kennicott River, Alaska: evidence for subglacial water storage cycles. Chem. Geol. 202, 297-312.

Anderson, S.P., 2004. Glaciers show direct linkage between erosion rate and chemical weathering fluxes. Geomorphology 67 (1-2): 147-157.

Andrews, J.T., Principato, S.M., 2002. Grain-size characterization and provenance of ice-proximal glacial marine sediments. Geological Society of America Special Publications 203, 305-324.

Asadov, A., Krofcheck, D., Gregory, M., 2001. Application of g-ray spectrometry to the study of grain size distribution of beach and river sands. Mar. Geol. 179, 203-211.

Augustsson, C., Fanning, M., Munker, C., Bahlburg, H., Jacobsen, Y., 2003. Sediment sources for the Late-Paleozoic SW South American Gondwana margin: Insights from U-Pb ages and Hf isotope compositions of single detrital zircons. Geological Society of America. 35, 390pp.

Ayres, A., Theilen, F., 2001. Natural gamma-ray activity compared to geotechnical and environmental characteristics of near surface marine sediments. J. Appl. Geophys. 48, 1-10.

Basu, A., 2002. A perspective on quantitative provenance analysis; Memorie Descrittive della Carta. Geologica d'Italia 61, 11-22.

Blum, J.D., 1995. Isotope Decay Data. In: Ahrens, T. J. (Ed.), Global Earth Physics, A Handbook of Physical Constant. A.G.U, pp. 271-282.

Blum, J.D., Erel, Y., 1997. Rb-Sr isotope systematics of a granitic soil chronosequence; the importance of biotite weathering. Geochim.Cosmochim. Acta 61, 3193-3204.

Boggs, S. Jr., 2001. Principles of Sedimentology and Stratigraphy, third ed. Prentice-Hall, New Jersey.

Brownlow, A.H., 1996. Geochemistry, second ed. Prentice-Hall, New Jersey.

Bruns, T.R., Schwab, W.C., 1983. Structure maps and seismic stratigraphy of Yakataga segment of the continental margin, northern Gulf of Alaska. Miscellaneous Field Studies Map - U. S. Geological Survey. Report: MF-1424, 20.

Calkin, P.E., Wiles, G.C., Barclay, D.J., 2001. Holocene coastal glaciation of Alaska; Quatr. Sci. Rev. 20, 449-461.

Carter, R.M., Gammon, P., 2004. New Zealand Maritime glaciation: Millennium-scale southern climate change since 3.9 Ma. Science 304, 1659-1662.

Collins, D.N., 1979. Hydrochemistry of meltwaters draining from an alpine glacier. Arctic and Alpine Res. 11, 307-323.

Cowan, E.A., Powell, R.D., Smith, N.D., 1988. Rainstorm-induced event sediment at the tidewater front of a temperate glacier. Geology 16, 409-412.

Curran, K.J., Hill, P.S., Milligan, T.G., Cowan, E.A., Syvitski, J.P.M., Konings, S.M., 2003. Fine-grained sediment flocculation below the Hubbard Glacier meltwater plume, Disenchantment Bay, Alaska. Mar. Geol. 203, 83-94.

Cutshall, N.H., Larsen, I.L., Olsen, C.R., 1983. Direct Analysis of Pb-210 in sediment samples – self-absorption corrections, Nuclear Instruments and Methods. Physics Res. 206 (1-2), 309-312.

Derry, L.A., France Lanord, C., 1996. Neogene Himalayan weathering history and river (super 87) Sr/ (super 86) Sr; impact on the marine Sr record. Earth Planetary Sci. Letters 142, 59-74.

Dessert, C., Dupre, B., Gaillardet, J., Francois, L.M., and Claude, J.A., 2003. Basalt weathering laws and the impact of basalt weathering on the global carbon cycle. Chem. Geol. 202, 257-273.

Dobson, M.R., O'Leary, D., Veart, M., 1998. Sediment delivery to the Gulf of Alaska: source mechanisms along glaciated transform margin; In: Stocker, M.S., Evans, D., Cramp, A. (Eds.), Geological Processes on Continental Margins: Sedimentation, Mass-Wasting and Stability. Geological Society, London, Spec. Pub. 129, pp. 43-66.

Doveton, J.H., 1994. Geologic log interpretation; SEPM Short Course, 169, Society of Sedimentary Geology, Tulsa, OK, United States (USA).

Duval, J.S., Cook, B., Adams, J.A.S., 1971. Circle of investigation of an air-borne gamma-ray spectrometer; J. Geophys. Res. 76, 8466-8470.

Duval, J.S., 2001. Aerial Gamma-Ray Surveys in Alaska. U.S. Geological Survey Open File Report 01-128.

Fabres, J., Calafat, A., Canals, M.A., Barcena, M.A., Flores, J.A., 2000. Bransfield Basin fine-grained sediments; late-Holocene sedimentary processes and Antarctic oceanographic conditions. The Holocene, 10, 703-718.

Faure, G., 1986. Principles of Isotope Geochemistry, Wiley, New York.

Fedo, C.M., Eriksson, K.A., Krogstad, E.J., 1996. Geochemistry of shales from Archean (approximately 3.0 Ga) Buhwa greenstone belt, Zimbabwe; implications for provenance and source-area. Geochim. Cosmochim. Acta 60, 1751-1763.

Flemings, P.B., Behrmann, J.H., John, C.M., and the Expedition 308 Scientists 2006. Methods, In: Proc. IODP, 308: College Station TX (Integrated Ocean Drilling Program Management International, Inc.) doi:10.2204/iodp.proc.308.102.2006.

Fralick, P., 2003. Geochemistry of clastic sedimentary rocks: ratio techniques; In: Lentz, D.R. (Ed), Geochemistry of Sediments and Sedimentary Rocks: Evolutionary Considerations to Mineral Deposit-Forming Environments; Geological Association of Canada. Geotext 4, pp. 85-103.

Goldfarb, R.J., Borden, J.C., 1992. Geochemical evaluation of stream-sediment data from the Bering Glacier and Icy Bay quadrangles, south-central Alaska; U. S. Geological Survey Bulletin. Report: B 2068, pp. 178-186.

Gustavson, T.C., Boothroyd, J.C., 1982. Subglacial fluvial erosion; a major source of stratified drift, Malaspina Glacier, Alaska. Guelph Symposium on Geomorphology 6, pp. 93-116.

Hallet, B., Hunter, L., Bogen J., 1996. Rates of erosion and sediment evacuation by glaciers: A review of field data and their implications. Global Planetary Change 12, 213-235.

Hamilton, T.D., 1994. Late Cenozoic glaciation of Alaska, In: Plafker, G., Berg, H.C. (Eds.), The Geology of North America, v. G-1, The Geology of Alaska. Geological Society of America, Boulder, CO.

Harlavan, Y., Erel, Y., 2002. The release of Pb and REE from granitoids by the dissolution of accessory phases. Geochim. Cosomochim.Acta 66, 837-848.

Hein, J.R., Dowling, J.S., Schuetze, A., Lee, H.J., 2003. Clay-mineral suites, sources and inferred dispersal routes: Southern California continental shelf. Mar. Environmental Res. 56, 79-102.

Hill, P.S., Syvitski, J.P.M., Cowan, E.A., Powell, R.D., 1998. In situ observations of floc settling velocities in Glacier Bay, Alaska. Mar. Geol. 145, 85-94.

Hillhouse J.W., Coe, R.S., 1994. Paleomagnetic data from Alaska, In: Plafker, G., Berg, H.C., (Eds.) The Geology of North America, v. G-1, The Geology of Alaska. Geological Society of America, Boulder, CO.

Hodson, M.E., 2002. Variation in element release rate from different mineral size fractions from the B horizon of a granitic podzol – size is important. Chem. Geol. 190, 91-112.

Hounslow, M.W., Morton, A.C., 2004. Evaluation of sediment provenance using magnetic mineral inclusions in clastic silicates: comparison with heavy mineral analysis. Sediment. Geol. 171, 13–36.

Hunter, L.E., Powell, R.D., Lawson, D.E., 1996. Flux of debris transported by ice at three Alaskan tidewater glaciers. J. Glaciology 42, 123–135.

Hurst, A., 1990. Natural gamma-ray spectrometry in hydrocarbon-bearing sandstones from the Norwegian Continental Shelf, In: Hurst, A., Lovell, M.A., Morton, A.C. (Eds), Geological Application of Wireline Logs, Geological Society of London Spec. Pub. 211-222.

Hutchison, S.G., Hutchison, F.I., 1997. Radioactivity in Everyday Life. J. Chem. Education 74, 503pp.

Irwin, R.J., VanMouwerik, M., Stevens, L., Seese, M.D., Basham W., 1997. Environmental Contaminants Encyclopedia. National Park Service, Water Resources Division, Fort Collins, CO. Distributed within the Federal Government as an electronic Document (Projected public availability on the internet or NTIS: 1998).

Jaeger, J.M., Nittrouer, C.A., Scott, N.D., Milliman, J.D., 1998. Sediment accumulation along a glacially impacted mountainous coastline: north-east Gulf of Alaska. Basin Res. 10 (1), 155-173.

Jaeger J.M., Nittrouer, C.A., 1999. Sediment deposition in an Alaskan Fjord: Controls on the formation and preservation of sedimentary structures in Icy Bay. J. Sediment. Res. 69, 1011-1026 Part A.

Jaeger, J.M., Hallet, B., Pavlis, T., Sauber, J., Lawson, D., Milliman, J., Powell, R., Anderson, S. P., Anderson, R., 2001. Orogenic and glacial research in pristine southern Alaska. Eos Transactions, American Geophysical Union. 82, pp. 213-216.

Jaeger, J.M., 2002. Developing high resolution chronologies in glacimarine sediments: examples from southeastern Alaska, In: Dowdeswell, J.A., O'Cofaigh, C. (Eds.), Glacier-Influenced Sedimentation on High-Latitude Continental Margins. Geological Society, London, Spec. Pub. 203, pp. 195-213.

Jaeger, J.M., Nittrouer, C.A., (accepted). A quantitative examination of modern sedimentary lithofacies formation on the glacially influenced Gulf of Alaska continental shelf. Continental Shelf Res.

Kairyte, M., Stevens, R.L., Egidijus, T., 2005. Provenance of silt and clay within sandy deposits of the Lithuanian coastal zone (Baltic Sea). Mar. Geol. 218, 97-112.

Kampunza, A.B., Cailteux, J.L.H., Moine, B., Loris, H.N.B.T., 2005. Geochemical characterization, provenance, source and depositional environment of 'Roches Argilo-Talqueuses' (RAT) and Mines Subgroups sedimentary rocks in the Neoproterozoic Katangan Belt (Congo); Lithostratigraphic implications. J. African Earth Sci. 42, Issues 1-5, 119-133.

Kusky, T.M., Bradley, D.C., Donley, D.T., Rowley, D., Haeussler, P., 2003. Controls on intrusion of near-trench magmas of the Sanak-Baranof belt, Alaska, during Paleogene ridge subduction, and consequences for forearc evolution, In: Sisson, V.B., Roeske, S., Pavlis, T.L. (Eds.), Geology of a Transpressional Orogen Developed During a Ridge-Trench Interaction Along the North Pacific Margin. Geol. Soc. America Spec. Paper 371, pp. 269–292.

Lang-Farmer, G., Ayuso, R., Plafker, G., 1993. A coast Mountains provenance for the Valdez and Orca groups, southern Alaska, based on Nd, Sr, and Pb isotopic evidence. Earth Planetary Sci. Letters.

Lewis, D.W., McConchie, D., 1994. Analytical Sedimentology, Chapman and Hall, New York.

Liu, H., Zhu, R.X., Li, G.X., 2003. Rock magnetic properties of the fine-grained sediment on the outer shelf of the East China Sea: implication for provenance. Mar. Geol. 193, 195-20.

Lull, J.S., Plafker, G., 1989. Geochemistry and paleotectonic implications of metabasaltic rocks in the Valdez Group, southern Alaska, In: Dover, J.H., Galloway, J.P. (Eds.), Geologic studies in Alaska by the U.S. Geological Survey. U.S. Geol. Survey Bulletin 1946, pp. 29-38.

Martin, G.C., 1993. Lithostratigraphy, In: Risely, D.E. et al. (Eds.), Geologic Report for the Gulf of Alaska planning area. Mineral Management Service Report 92-0065, pp. 63-98.

Mazzotti, S., Hyndman, R.D., 2002. Yakutat collision and strain transfer along the northern Canadian Cordillera. Geology, Geological Society of America 30, pp. 495-498.

McDaniel, D.K., McLennan, S.M., Hanson, G.N. 1997. Provenance of Amazon Fan muds; constraints from Nd and Pb isotopes, In: Fox, G.L. (Ed.), Proceedings of the Ocean Drilling Program, Scientific Results 155, pp. 169-176.

McLennan, S.M., Taylor, S.R., Kroner, A., 1983. Geochemical evolution of Archean shales from South Africa; I, The Swaziland and Pongola supergroups. Precambrian Res. 22, no. 1-2, 93-124.

McLennan, S.M., Bock, B., Hemming, S.R., Hurowitz, J.A., Lev, S.M., McDaniel, D.K., 2003. The roles of provenance and sedimentary processes in the geochemistry of sedimentary rocks; In: Lentz, D.R. (Ed.), Geochemistry of Sediments and Sedimentary Rocks: Evolutionary Considerations to Mineral Deposit-Forming Environments, Geol. Assoc. Canada, Geotext 4, pp. 7-38.

Monger, J.W.H. Berg, H.C., 1984. Lithotectonic Terrane Map of Western Canada and Southeastern Alaska; U.S. Geological Survey. Open-file Report 84-523, Part B.

Molnia, B.F., Hein, J.R., 1982. Clay mineralogy of a glacially dominated, subarctic continental shelf; northeastern Gulf of Alaska. J. Sediment. Petrol. 52, 515-527.

Moore, D.M., Reynolds, R.C., 1997. X-Ray Diffraction and the Identification and Analysis of Clay Minerals, second ed. Oxford, New York.

Naidu, A.N., Han, M.W., Mowatt, T.C., Wajda, W., 1995. Clay minerals as indicators of sources of terrigenous sediments, their transportation and deposition: Bering Basin, Russia--Alaskan Arctic. Mar. Geol. 127, 87-104.

Nir-El, Y., 1997. Traceability in the amount-of-substance analysis of natural potassium, thorium and uranium by the method of passive gamma-ray spectrometry. Accreditation and Quality Assurance 2, pp. 193-198.

Nockleberg, W.J., Brew, D.A., Grybeck, D., Yeend, W., Bundtzen, T.K., Robinson, M.S., Smith, T.E., 1994. Metallogeny and major mineral deposits of Alaska, In: Plafker, G., Berg, H.C. (Eds.), The Geology of North America, v. G-1, The Geology of Alaska. Geological Society of America, Boulder, CO, pp. 855-903.

Nyakairu, G.W.A., Koeberl, C., 2001. Mineralogical and chemical composition and distribution of rare earth elements in clay-rich sediments from central Uganda. Geochem. J. 35, 13-28.

Plafker, G., 1997. Geology and petroleum potential of the northern Gulf of Alaska continental margin, In: Scholl, D.W., Grantz, A., Vedder, J.G. (Eds.), Geology and Resource Potential of the Continental Margin of Western North America and Adjacent Ocean Basins, Earth Science Services. Circum-Pacific Council for Energy and Mineral Resources 6, Houston, TX, p.229-268.

Plafker, G., Nockelberg, W.J., Lull, J.S., 1989. Bedrock geology and tectonic evolution of the Wrangellia, Peninsular, and Chugach terranes along the Trans-Alaska Crustal Transect in the Chugach Mountains and southern Copper River Basin, Alaska. J.Geophys. Res. 94, 4255-4295.

Plafker, G., Moore, J.C., Winkler, G.R., 1994. Geology of the southern Alaskan margin, In: Plafker, G., Berg, H.C., (Eds.), The Geology of North America, v. G-1, The Geology of Alaska, Geological Society of America, Boulder, CO, pp. 389-449.

Powell, R.D., 1984. Glacimarine processes and inductive lithofacies modeling of ice shelf and tidewater glacier sediments based on quaternary examples. Mar. Geol. 57, 1-52.

Powell, R.D., Molnia, B.F., 1989. Glacimarine sedimentary processes, facies and morphology of the South-Southeast Alaska shelf and fjords. Mar. Geol. 85 (2-4), 359-390.

Ruffell, A., Worden, R., 1999. Palaeoclimate analysis using spectral gamma-ray data from the Aptian (cretaceous) of southern England and southern France. Palaeogeography, Palaeoclimatology, Palaeoecology 155, 265-283.

Saltus, R.W., Riggle, F.E., Clark, B.T., Hill, P.I., 1999. Merged aeroradiometric data for Alaska: USGS Open File Report 99-0016.

Sauber, J., Molnia, B., 2003. Glacier ice mass fluctuations and fault instability in tectonically active southern Alaska. Global and Planetary Change, Topical Volume "Ice Sheets and Neotectonics" 42, pp. 279-293.

Sharma, G.D., 1979. The Alaskan shelf: Hydrographic, sedimentary, and geochemical environment, Springer-Verlag, New York.

Schnyder, J., Ruffell, A., Deconinck, J., Baudin, F., 2005. Conjunctive use of spectral gamma ray logs and clay mineralogy in defining late Jurassic-early Cretaceous paleoclimate change. Paleogeography, Paleoclimatology, Paleoecology 229, 303-320.

Stephansson, A., Gislason, S.R., Arnorsson, S., 2001. Dissolution of primary minerals in natural waters II, Mineral saturation state. Chem. Geol. 172, 251-276.

Syvitski, J.P.M., 1988. On the deposition of sediment within glacier-influenced fjords: Oceanographic controls. Mar. Geol. 85, 301-329.

Syvitski, J.P.M., 1991. Principles, Methods and Applications of Particle Size Analysis, Cambridge University Press, Cambridge.

Taboada, T., Cortizas, A.M., Garcia, C., Garcia-Rodeja, E., 2006. Particle-size fractionation of titanium and zirconium during weathering and pedogenesis of granitic rocks in NW Spain, GEODERMA 131 (1-2), pp. 218-236.

Taylor, S.R., McLennan, S.M., McCulloch, M.T., 1983. Geochemistry of Loess, Continental Crustal Composition and Crustal Model Ages. Geochim. Cosmochim. Acta 47, 1897-1905.

Turner, R.F. (Ed.), 1992. Geologic Report for the Gulf of Alaska Planning Area, OCS Report; MMS 92-0065.

Van Wagoner, J.C., 1990. Sequence boundaries in siliciclastic strata on the shelf; physical expression and recognition criteria. AAPG Bulletin 74, pp. 1774-1775.

Van Wijngaarden M., Venema, L.B., De Meijer, R.J., Zwolsman, J.J.G., Van Os, B., Gieske, J.M.J., 2002. Radiometric sand-mud characterisation in the Rhine-Meuse estuary - Part A. Fingerprinting. Geomorphology 43, 87-101(15).

Ward, L.G., Moslow, T.F., Finkelstein, K., 1987. Geomorphology of a Tectonically Active, Glaciated Coast, South-Central Alaska, In: Fitzgerald, D. M., and Rosen, P. S. (Eds.), Glaciated Coasts, Academic Press Inc., California, pp. 1-31.

Watkins, S.J., Maher, B.M., 2003. Magnetic characterisation of present-day deep-sea sediments and sources in the North Atlantic. Earth Planetary Sci. Letters 214 (3-4), pp. 379-394.

Weaver, T.A., (project manager) (1983). The Geochemical Atlas of Alaska; Geochemistry Group, earth and space sciences division; Los Alamos National Laboratory, Los Alamos, NM, (GJBX-32; LA-9897-MS UC-51).

Weltje, G.J., Eynatten, H., 2004. Quantitative provenance analysis of sediments: review and outlook. Sediment. Geol. 171, 1-11.

White, A.F., Blum, A.E., 1995. Effects of climate on chemical weathering in watersheds. Geochim. Cosmochim. Acta 59, 1729.

White, A.F., Blum, A.E., Bullen, T.D., Vivit, D.V., Schultz, M., Fitzpatrick, J., 1999. The effect of temperature on experimental and natural chemical weathering rates of granitoid rocks. Geochim. Cosmochim. Acta 63, 3277-3291.

BIOGRAPHICAL SKETCH

Alice Hildick was born in Vermont on February 16, 1979. She grew up in Florida, where she graduated from Clearwater Central Catholic High School. She got her bachelor's degree in geology from the University of Florida in 2001, worked for Geohazards, Inc., then returned to the University of Florida to get her Master of Science degree. She spent time working at GeoSierra, LLC in Atlanta for a brief period during her Masters research. Alice's favorite things include traveling, surfing, and wine.